Addis Ababa University
Addis Ababa Institute of Technology (AAiT)
School of Electrical and Computer Engineering
Microelectronics Engineering Stream

Analysis of the Effect of Presence of Magnetic Field in Photon-Electron Interface

A thesis submitted to School of Graduate Studies and Research in Partial Fulfillment of the Requirement for the Master's Degree

By
Alema Abraha

Advisor
Dr. Eng. Getachew Alemu

Addis Ababa, Ethiopia
November 15, 2021

Declaration

I, the undersigned, declare that this thesis work is my original work, has not been presented for a degree in this or any other universities, and all sources of materials used for the thesis work have been fully acknowledged.

Name: Alema Abraha

Signature: _____

Date: _____

This MSc. thesis has been submitted for examination with my approval as an advisor.

Advisor: Dr. Eng. Getachew Alemu

Signature: _____

Date: _____

Approval by Board of Examiners

---------- ----------

Chairman Signature

Dr. Eng. Getachew Alemu

---------- ----------

Advisor Signature

---------- ----------

Internal Examiner Signature

---------- ----------

External Examiner Signature

Acknowledgment

First and foremost, praises and thanks to the God, the Almighty to whom I owe my every existence, for the strengths, and His blessing in completing this thesis.

I am greatly thankful to my advisor Getachew Alemu (PhD.), for his unreserved support, professional guidance, and constant encouragement from the commencement of the study to completion of the thesis.

I am also grateful to Mr. Tesfaye Mamo, advanced optic lab assistant at Addis Ababa University, Arat Killo Physics Department, who helped me with experiments.

I would also like to express my thanks to Ethio-Telecom and Ethio-Telecom employees Addis and Tibebu, who delivered me some of the key devices used in the experiments.

Finally, I owe my deepest gratitude to my parents for their love and support.

Abstract

Electronics played a great role in storing, computing, and transmitting data. However, electronics had certain limitations in bandwidth, speed, power consumption, and electromagnetic interfering. Conversely, photonic provides advantages like large bandwidth, lower power consumption, and immune to electromagnetic interference. Therefore, to overcome the electronics limitations, electronics and photonics integration developed.

Despite many advantages of the integration of electronics and photonics, the presence of an external magnetic field in photon-electron interfaces influences the performances of lasers and photodiodes. Those effects are well studied when lasers and photodiodes are separately subjected to the magnetic field in previous studies. However, the difference in the magnetic field effects on the output signal when both transducers are concurrently exposed to the field needs further study. Additionally, the influence of change in input signal frequency to the magnetic field effect on output signal when laser and photodiode are separately and simultaneously exposed also needs further study.

To demonstrate the difference in magnetic field effect on the output signal when the frequency of input signal varies as well as both laser and photodiode concurrently exposed to magnetic field relative to separately subjected; experimental setup was prepared in the laboratory by connecting VCSEL and PIN photodiode with other devices. Then experiments were conducted at around room temperature. During experimentation, both transducers were individually and concurrently exposed to the static magnetic field oriented $\boldsymbol{B//n}$ and $\boldsymbol{B^{\perp}n}$, at 3 kHz & 10 kHz. Then output voltage was measured and recorded at 0, 400, 600, 800, and 1000mT.

The results were compared based on the rate of change in output voltage at different magnetic flux densities and frequencies. The magnetic field effect on output signal was found higher at 3 kHz compared to at 10 kHz for both VCSEL and PIN photodiode individually and concurrently exposed. Additionally, the comparisons made at a fixed frequency showed that the magnetic field effect on output signal was much higher when VCSEL and PIN photodiode concurrently exposed relative to individually exposed.

Key words: Photon-electron interface, Semiconductor Lasers, Photodiodes, Magnetic field

Table of Contents

List of Figures

List of Tables

List of Acronyms and Abbreviations

MOS	Metal-Oxide Semiconductor
IC	Integrated Circuit
CMOS	Complementary Metal-Oxide-Semiconductor
VLSI	Very-Large-Scale-Integration
PIC	Photonic Integrated Circuit
WDM	Wavelength-Division Multiplexing
MZI	Mach Zehnder Interferometer
LASER	Light Amplification by Simulated Emission of Radiation
F.P.	Fabry-Perot
VCSEL	Vertical Cavity Surface Emitting Laser
DFB	Distributed Feedback
DBR	Distributed Brag Reflector
QWL	Quantum Wall Laser
APD	Avalanche Photodiode
n_A	Air Refractive Index
n_G	Glass Refractive Index
ISI	Inter-Symbol Interference
PSP	Principal State of Polarization
DGD	Differential Group Delay
PMD	Polarization Mode Dispersion
SOI	Silicon on Insulator
n	Refractive Index
B	Magnetic Flux Density
T	Temperature
I	Current
UV	Ultra-violate
IR	Infrared
EM	Electromagnetic

Chapter 1

Introduction

1.1 Background

1.1.1 Electronics

The field of electronics was born in 1883 at the time Thomas Edison discovered an electron tube. In his experimentation, Edison put a strip of metal inside a vacuum glass bulb with filament between metal strips and connected an ammeter to one of the filament contacts and found that electrons would flow by ammeter when the filament remained hot and stopped when the filament get cooled. The white-hot filament in the lamp was freeing electrons into the vacuum. Those electrons were returning to the metal strip through the galvanometer and back to the filament [1].

Later, Lee De Forest developed a sort of vacuum tube that was able to amplify radio signals based on the Thomas Edison principle in 1906. This invention endorsed the development of radio broadcasting, the telephone, television, and the first digital computers. These primary electronic computers were large-size vacuum-tube systems, and the best-known type is the Electronic Numerical Integrator and Computer [1].

When engineers tried to build multifaceted circuits using the vacuum tube, they quickly became conscious of its limitations. These inadequacies interested scientists at Bell Laboratories to seek an alternative to the vacuum tube, and that led to the development of the transistor; William Shockley and his colleagues invented the transistor in 1947 at Bell Laboratories [2]. This invention enabled electronic circuits to become smaller, lower power, and more reliable than vacuum tube technology. For this invention, Shockley and two Bell Labs colleagues John Barden and Walter Brattain awarded the Nobel Prize a decade later. This breakthrough was quickly followed by the invention of planar transistors by Jack Kilby, a research engineer at Texas Instruments, in the late1950s [3]. He introduced the concept of integrating device and circuit elements onto a single silicon chip, and it was the origin of the density doubling law known as Moore's Law [4]. Integrated circuits with planar transistors extended operating and cost benefits of transistors to mass-produced electronic circuits laying the foundations for the field of microelectronics [5].

As the requirement of electronic applications increased, Gordon Moore recognized that product developments were needed for transistor integration. Metal-oxide semiconductor (MOS) technology [6] appeared as the most effective technique for achieving scales of integration [7]. During this time, the most significant product to be introduced was the microprocessor [8] and started the tremendous coupling of integrated circuit (IC) and software. However, power dissipation was becoming a significant issue by the mid-1980s, and the solution was to use a complementary metal-oxide-semiconductor (CMOS) technology. This technology reduces the reserve power loss in logic circuits to almost zero [7] and quickly became the standard for a very-large-scale- integration (VLSI). Following Moore's Law, over the years, the dimensions of the transistor have reduced from 10s of microns to 10 nanometers [9].

1.1.2 Photonics

Photonics is a technology related to signal generation, processing, transmission, and detection where the signal is carried by photons [10]. The word photonics is first used to elect a field of research part accountable to do tasks using light that is conventionally associated with the traditional field of electronics like telecommunications, information processing, and so on. The researches in the photonics field were initiated in 1960, after the discovery of laser. The advancement followed, with fiber optic communication, laser diode in the 1970s, and erbium fiber amplifiers. These developments made the foundations for the industrial revolution in the telecommunication sector during the last 20th century and delivered the internet infrastructure [10]. Fiber optics has played the main role in initiating the information age and changed the way information receive and communicate [5].

1.1.2.1 Photonic Integrated Circuit

The photonic integrated circuit (PIC) is a device that incorporates many photonic functions to perform certain operations into optical signals. In PIC for chip-to-chip as well as on-chip photonic interconnect communication, various components are needed. Those are lasers, modulators, waveguides, optical amplifiers, Wavelength-Division Multiplexing (WDM), photo detectors, and so on [11]. WDM applies many data channels in the same fiber or waveguide at different wavelengths [12]. The figure below shown Multi-wavelength rays propagated in a single waveguide by wavelength division multiplexing (WDM).

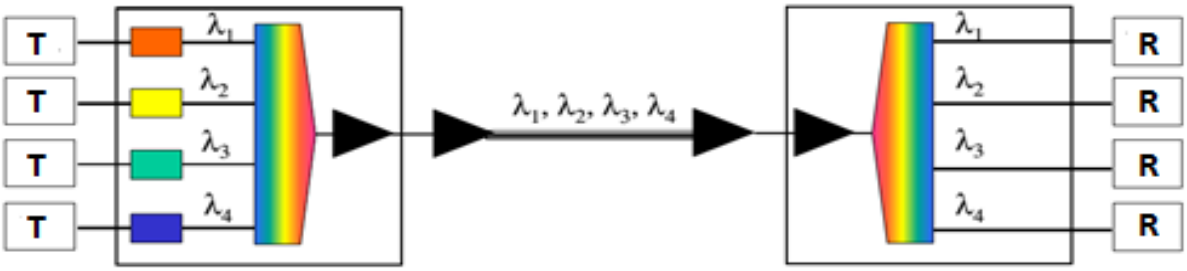

Figure1.1: WDM system. [13]

Most photonic integrated circuits, either for signal processing or data transfer, use the same fundamental components. The components used for optical signal processing are waveguides, splitters, fiber couplers, and so on. In photonic integrated circuits, electro-optic modulators, Mach Zehnder Interferometer (MZI), and ring resonators use to build photonic switches, filters, and modulators [14]. Figure1.2 shows, a voltage (V_{gate}) induced free carrier change ($n_{carrier}$) leads to a shift of the active material's relative permittivity ($\Delta\varepsilon_r(\omega)$, with ω the angular frequency) and consequently shift the real and imaginary part ($\Delta\kappa$) of the propagating modal index.

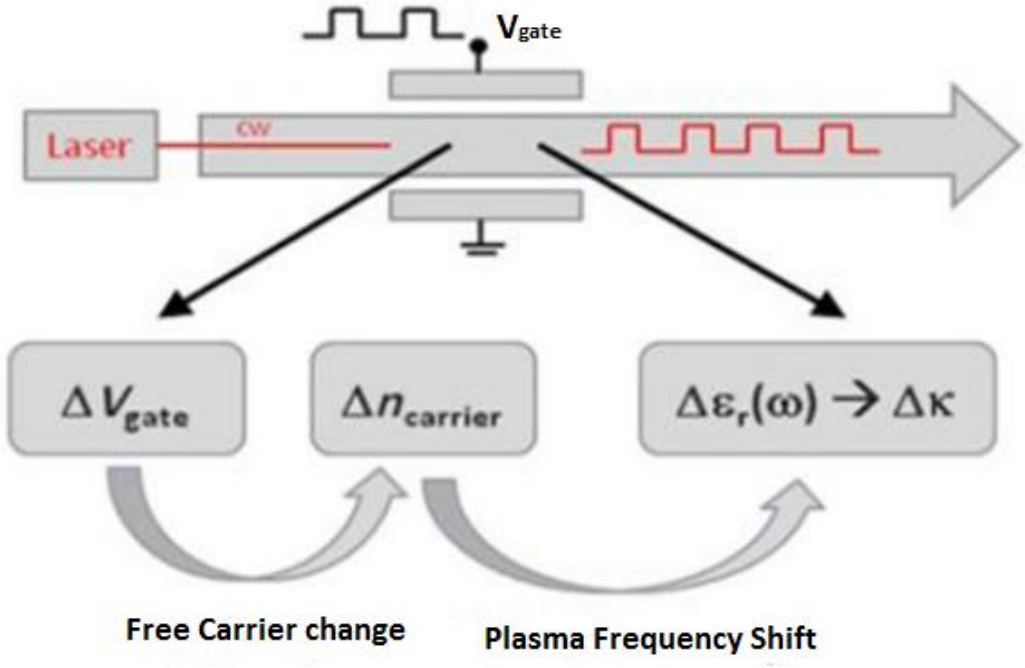

Figure1.2: Optical Modulation of data switching for integrated circuits with electro-optic modulator. [15]

1.1.3 Integration of Electronics and Photonics

Electronic-photonic integration deals with the application of electronic integrated circuits as well as photonic integrated circuits. Electronic devices are concerned with applying the properties of

electrons, and optical devices are used to process, transport, and generate photons. In electronic-photonic integrated systems, electronic devices offer extremely high density, and memories are easily constructed. Photonics enables high bandwidth and can operate at frequencies of several orders of the scale higher than electronics. It has enabled the demonstration of circuits with record functionalities such as high-speed internet, wireless communication with ultra-high data rates, and high-performance computing, some of the advanced achievements through the unique combination of both technology [5].

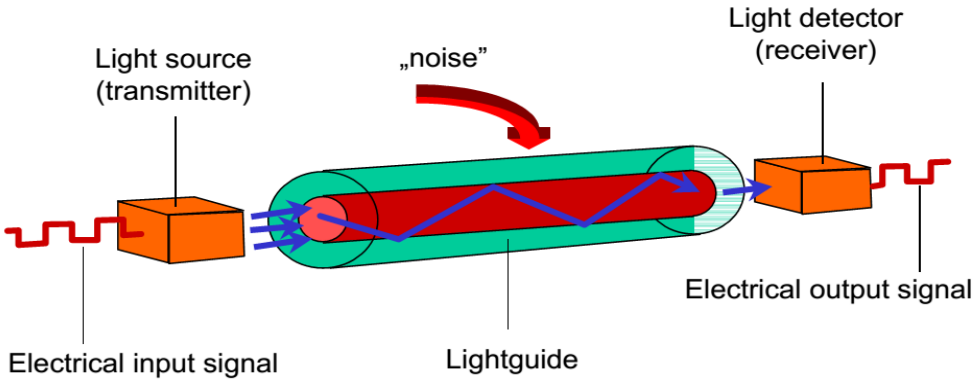

Figure 1.3: Schematic diagram of fiber optic system. [13]

1.1.3.1 Electronic-Photonic Integrated Chip

The scaling of CMOS transistor technology in the past few decades has led to significant enhancement in the speed of microprocessors. However, the bottleneck begins to change towards the data transport aspects from board to board, chip to chip, to continue with speed to feed the information. Therefore, as the demand for such on-chip functionality continues to grow, it is recognized that electronics technology increasingly requires integration with photonics to keep up with Moore's Law scaling [16], either through monolithic or heterogeneous integration. Today, high-speed data transmission over a bit rate of 10 GB/s makes photonic interconnects a calmer approach to implement than electrical interconnects [17].

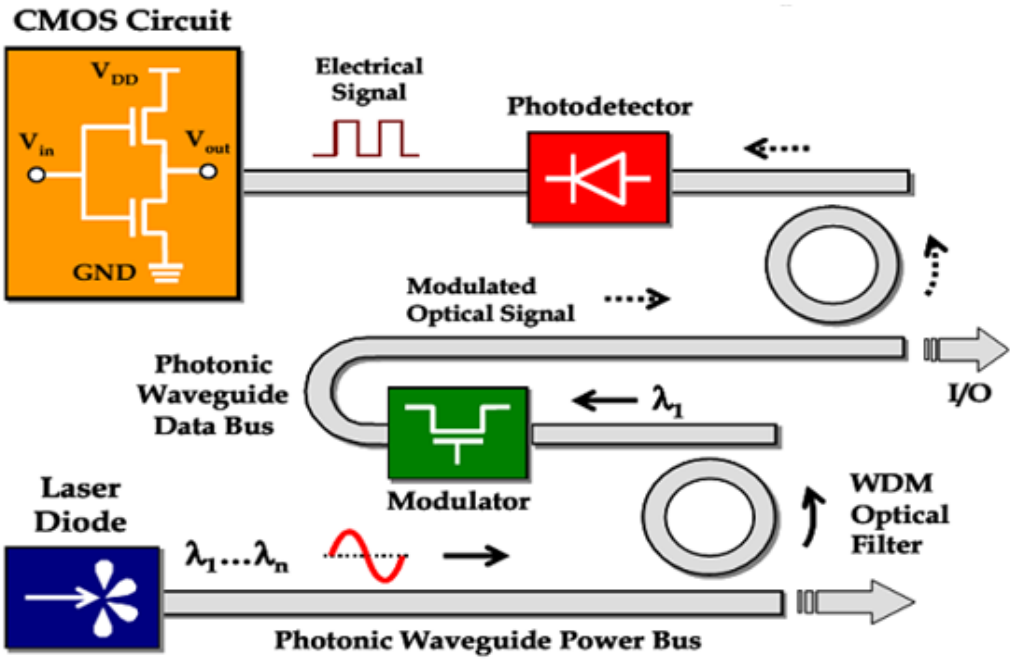

Figure 1.4: Schematic illustration of optical interconnects technology using the Si photonics platform and its convergence with an electronic integrated circuit. [17]

In an electro-photonic integrated chip, the photonic micro-waveguide made of Si core and oxide cladding is used to route the optical signal with low propagation loss. To upsurge the interconnect capacity, wavelength division multiplexing (WDM) provides multiple channel transmission for parallel data processing. The optical filter filters selected wavelength (λ_n) into the photonic waveguide data bus. While Silicon shows weaker electro-optical coefficients because of its central symmetry in the lattice structure, the free carrier plasma dispersion effect enables effective optical modulation in a phase-shifter. The modulated optical signals are channeled through the photonic waveguide data bus, and multiple wavelength signals deliver on the same channel without interfering with each other. At the receiver side, a signal with a specific wavelength is filtered and fed into a high-performance photo detector for enabling effective optical-to-electrical conversion. Then the electrical signal passes through CMOS logic circuitry for data processing [17].

1.2 Statement of the Problem

Several types of research have been done on electronics, photonics, and their integrations highly contributed to currently existing technologies used in various applications (telecommunication, military, space, medical, and so on). Those many technologies that have the photon-electron

interface consist of different types of transducers (lasers and photodiodes) to convert the electrical signal to an optical signal and vice versa and waveguides to carry an optical signal. However, the presence of a magnetic field on those interfaces influences the performances of transducers and causes changes in the laser's output signal characteristics (intensity, frequency, and wavelength) [18] - [21] and both dark and light currents of photodiode [22]. The effects depend on transducers type, the magnetic field strength, the field direction, and temperature.

The many research findings showed that the external magnetic field influences the performances of transducers used in photon-electron interfaces and causes effects on output signal characteristics. However, the difference in the magnetic field effects on the output signal relatively when both transducers (laser and photodiode) are concurrently exposed still requires further study, and this thesis study presented the difference in the effects. Additionally, the changes in input signal frequency could influence the rate of magnetic field effect on output signal when both laser and photodiode are individually and concurrently exposed to the magnetic field, and this scenario is also studied.

1.3 Objectives

1.3.1 General Objective

The main goal of this thesis is to investigate the phenomena at photon-electron interfaces and to identify the effect of the presence of a magnetic field on the photon-electron interface.

1.3.2 Specific Objectives

1. To identify the effect on the output signal when laser exposed to magnetic field.
2. To analyze the influence of changes in input signal frequency to magnetic field effect on output signal when laser exposed to magnetic field.
3. To identify effect on output signal when photo diode exposed to magnetic field.
4. To analyze the influence of changes in input signal frequency to magnetic field effect on output signal when photodiode exposed to magnetic field.
5. To identify the difference in magnetic field effect on output signal when both laser and photodiode are concurrently exposed to magnetic field relative to individually exposed.
6. To study the influence of changes in input signal frequency to magnetic field effect on output signal when both laser and photodiode are concurrently exposed to magnetic field.
7. To extract measuring parameters for comparison.

8. Comparison and analysis based on the result obtained from each experiment and giving the concluding results.

1.4 Significance of the Thesis

Nowadays, the combination of photonics and electronics technology becomes crucial in various applications due to its advantages and is expected to advance in the future. The outcome of this study identifies the magnetic field effects on the transducers used in the photon-electron interface. Especially the difference in output signal when both laser and photodiode concurrently exposed relative to individually exposed is analyzed. Additionally, the influence of change in input signal frequency to the magnetic field effect on output signal when laser and photodiode simultaneously and separately subjected to magnetic field studied. Moreover, this study gives insight for further research to analyze the magnetic field effect on different types of transducers used in photon-electron interfaces.

1.5 Scope and Limitations of the Thesis

This thesis focused on experimentation to identify the effect on output signal when transducers (laser and photodiode) are used in the photon-electron interface exposed to the magnetic field. Furthermore, the influence of change in input signal frequency to the magnetic field effect on output signal when laser and photodiode simultaneously and separately subjected to the magnetic field demonstrated. The awareness of this thesis study is to identify the magnetic field effect on output signal when the transducers used in the photon-electron interface are exposed.

Even though different types of lasers and photodiodes are being used in the photon-electron interface, only VCSEL and PIN photodiode was used in the experimentation due to resource limitation.

1.6 Literature Review

In various literatures described that the presence of the magnetic field in the photon-electron interface influences the performances of transducers (lasers and photodiodes) and causes a change in output signal characteristics. This section presented the effect of the magnetic field on semiconductor lasers and photodiodes.

Y. Yamagishi et al. studied the effects of the external magnetic field on Vertical Cavity Surface Emitting Laser (VCSEL) to identify the changes in output signal wavelength and frequency [18].

They experimented by exposing 850nm VCSEL to a field oriented perpendicular as well as parallel to VCSEL's layered surface at room temperature, the magnetic field strength 0.1 - 0.5T. Their results from the field-oriented perpendicular to VCSEL's layered surface showed that when field strength higher above 0.3T, a wavelength shifted toward the shorter wavelength side and intensity increased, and at 0.5T frequency shifted by 1.2 GHz toward the higher frequency side. The authors stated that the magnetic field oriented perpendicular to VCSEL layered surface boosts the carrier density in the active region, and that caused a shift in both wavelength and frequency. For magnetic field oriented parallel to VCSEL's layered surface, neither wavelength shift nor frequency shift was evident.

The study made on the performance of a Distributed Feedback (DFB) laser under the external magnetic field demonstrated by J. Troska et al. indicated that the DFB laser is sensitive to the external magnetic field [19]. They subjected a 1310nm DFB laser to an external magnetic field oriented perpendicular to the DFB laser's layered surface between 0 - 2T and at 0.7T parallel to the DFB laser's layered surface. Their result showed that the optical power decreased when the strength of the magnetic field perpendicular to the DFB laser's layered surface increased, and no change in optical power was observed for the field directed parallel to the DFB laser's layered surface.

Tho-Alfiqar and Aurangzeb Khurram studied the effects on the output power of around 668nm AlGaInP MQW laser under the influence of a low external magnetic field at the range of 0 - 2T [20]. The results from their experiment at T = 35^0C showed that output power dropped from 574.2 to 481.4 µW for the magnetic field directed perpendicular to the MQ plane and 574.2 to 555 µW for the magnetic field direction parallel to the MQ plane. The authors specified that the reason for decreasing in output power was the magnetic field suppresses the recombination rate of the diffusing charge carriers due to thermal agitation having momentum in the direction normal to the magnetic field.

Later, another study made by Samer and Atef to demonstrate the influence of magnetic field in pulse distribution and intensity of 670 nm AlGaInP MQW laser also showed that significant changes in the pulse form and intensity [21]. The experiment was conducted at T = 300K by varying magnetic field between 0 to 0.55T, oriented perpendicular and parallel to the laser's layered surface. The result showed that dropping in the top of the pulse, pulse form distortion by

the appearance of the number of peaks and dips of the pulse, and decreasing intensity for both perpendicular and parallel orientation of the magnetic field. The authors stated that the magnetic field suppressed the propagation current due to the Lorentz force. That induced change in the current flow and increased current density in the active region resulted in a change in pulse form. The magnetic field influenced the mechanisms of loss in the laser gap and led to changes in the current density and thus affected the temperature near the active area and resulted in intensity reduction.

The research has been done to identify the responsivity of a silicon photodiodes dark and light current under the influence of the magnetic field and temperature by Sawsan Ahmed et al. [22], shown that the external magnetic field and temperature affect the performances of a silicon photodiode. They subjected silicon photodiode to the magnetic field and measured output voltage and current varying magnetic field strength. Their results showed that both dark and light current increased while the magnetic field increased and decreased, whereas temperature increased. The authors stated that the magnetic field raised the energy gained by the free carriers, and that caused increases in both dark and light current in silicon photodiodes.

Several types of research presented the effect of the presence of a magnetic field on the performances of different types of transducers used in the photon-electron interface when they are individually exposed to the magnetic field. In the present thesis work, the difference in the effects on the output signal when both transducers (laser and photodiode) are concurrently exposed to the magnetic field comparative to both transducers individually exposed studied. Additionally, the difference in magnetic field effect on output signal when both laser and photodiode individually and concurrently exposed at a different frequency studied.

1.7 Organization of the Thesis

The rest of this thesis is organized into the following chapters; in Chapter-2, the fundamentals of optical devices and waveguides are discussed. Chapter-3 explains waveguides loss and the effects of magnetic field on semiconductor lasers and photodiodes, and Chapter-4 describes the method, experimental setup arrangement, and experiments conducted for effective measurement. Chapter-5 presents results accompanied by useful discussions. Chapter-6 offers a conclusion and recommendations for possible future work.

Chapter 2

Optical Devices and Waveguides

2.1 Semiconductor Lasers

Light amplification by stimulated emission of radiation (LASER), as its name suggests that the stimulated emission is the basic phenomenon involves in the operation of the laser. In semiconductor lasers, mainly three processes occur. The first process is absorption, and in which electrons in the valance band are excited by absorbing a photon with energy equal to the optical band gap and promoted to the conduction band. In the second process, spontaneous emission occurs when an electron in the conduction band with energy E_2 recombines with a hole in the valance band at a lower energy E_1. The difference in E_2-E_1 radiated in photon form. This process is random, and photons are emitted in any direction with arbitrary polarization. The third process is stimulated emission and happens when photons of energy E_2-E_1 interact with an electron in the conduction band and recombine with a hole producing a photon. The photon released by this process has identical energy, phase, and momentum to that of the incident photon [23].

2.1.1 Fabry-Perot (F.P.) Laser

Fabry-Perot laser is a sort of semiconductor laser in which the two parallel ends of the semiconductor are cleaved lengthwise crystal axis, creating reflective mirrors forming the laser cavity with the semiconductor as the gain medium. The optical coating applied to the mirror surfaces to optimizing the output power with the laser emission taken from the low reflectivity front facet and high reflectance on the back to decrease the total mirror loss. The gain spectrum is quite wide and supports lasing over many longitudinal modes of the laser cavity. Consequently, this kind of laser typically operates with multiple longitudinal modes [24].

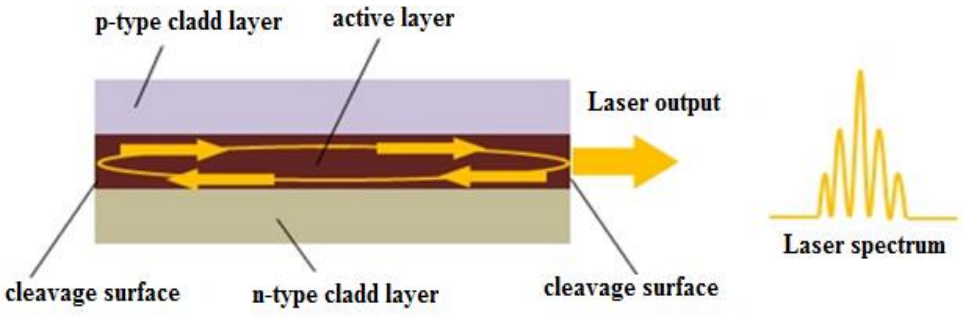

Figure 2.1: Fabry-Perot laser diode. [25]

2.1.2 Vertical Cavity Surface Emitting Laser (VCSEL)

In a VCSEL, the cavity length is made very short, and the laser beam is emitted perpendicular to the wafer and in the same direction as the injected current. Because VCSEL emits from its surface and the optical cavity in which optical field experience gain is very short. The optical field requires making several passes through the active region and needs highly reflective end mirrors to reach the threshold gain level [23]. In this sort of laser, the active layer is sandwiched among a stack of Bragg mirrors, which are alternate layers of high and low refractive-index materials, designed to be quarter wavelengths thick at the desired laser wavelength. The Bragg mirrors provide very high reflectivity of the light back into the active region, allowing the VCSEL to generate a sufficient gain [26].

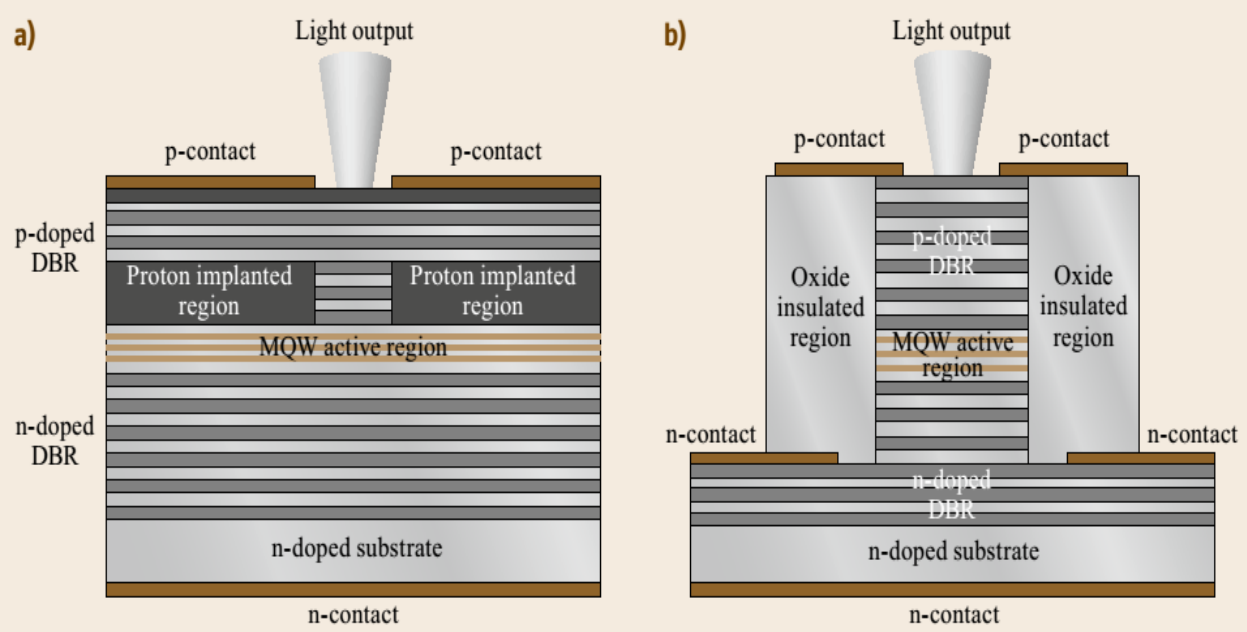

Figure 2.2: Cross-sections of two common cylindrical VCSEL (a) a proton-bombarded top-bottom contact design and (b) an oxide confined side-contact design. [23]

2.1.3 Distributed Feedback (DFB) Laser

In the DFB laser, there is a corrugated structure overhead of the laser active layer, which is a zig-zaggy composition. This combination of refractive index and the space of corrugations serve to reflect only a specific wavelength of light. Light traveling in the active layer goes in all directions and finally strikes the upper surface of the active layer hits zig-zag. In this way, the corrugations act as a grating and reflect only a particular wavelength into the cavity but allow others to pass through. The feeding-back the wanted wavelength into the cavity takes place over

the whole length of the laser, and the only light that builds up in the active layer with a specific wavelength is outputted [27].

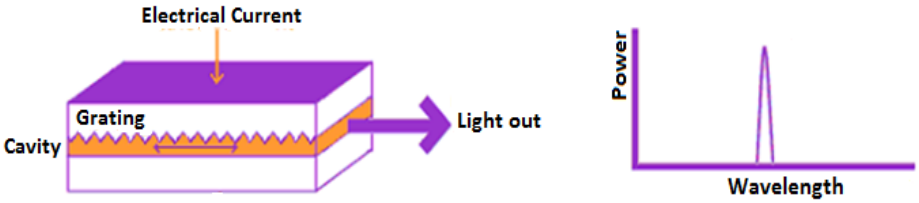

Figure 2.3: DFB laser. [27]

2.1.4 Quantum Well Laser (QWL)

A quantum well is a potential well that confines particles that are initially free to mobile in three dimensions to two and force them to inhabit a planar region. The quantum confinement happens when the QW thickness becomes equivalent to or smaller than the de Broglie wavelength of the carriers. In a QW, the energy band leads to energy levels termed energy sub-bands, and which means the carriers can only have discrete energy values perpendicular to the potential well and parallel to the well [28].

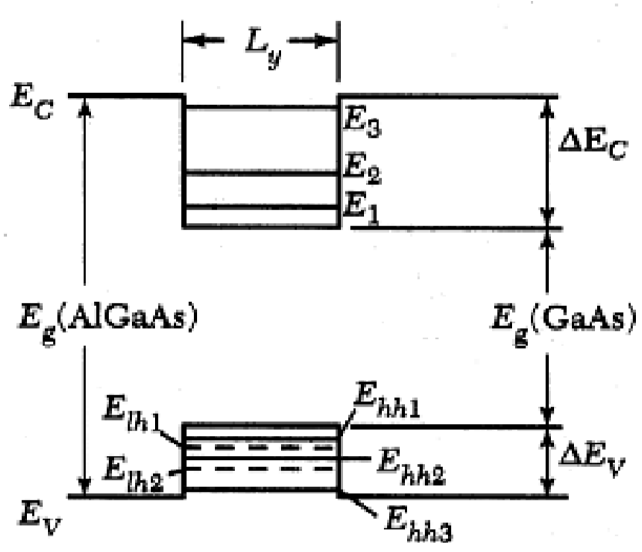

Figure 2.4: Quantum well structure. [29]

In a QW laser, the group of electrons and holes with nearly the same energy recombines. For example, the recombination of the level E_l in the conduction band and the level E_{hhl} in the valence band is shown in figure 2.4. QW lasers offer a significant improvement in laser performance, such as the reduction in the threshold current, high output power, and high speed, compared with the conventional DH lasers [29].

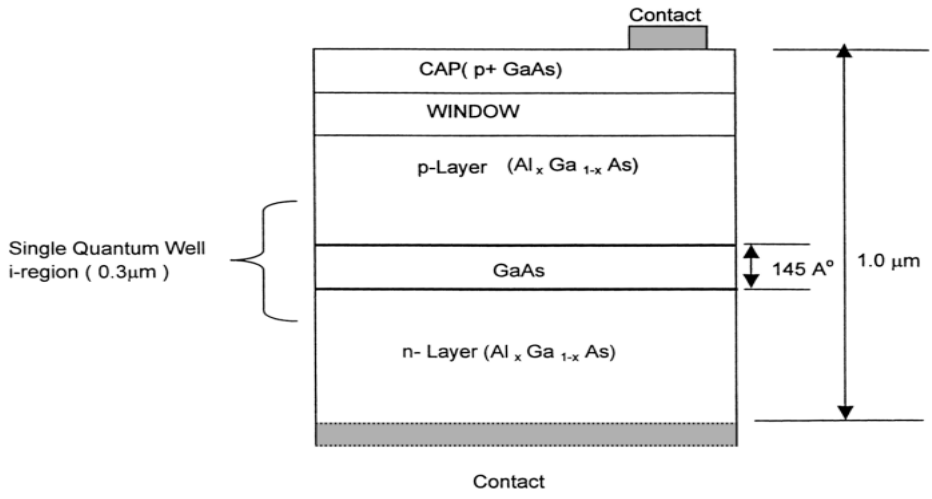

(a)

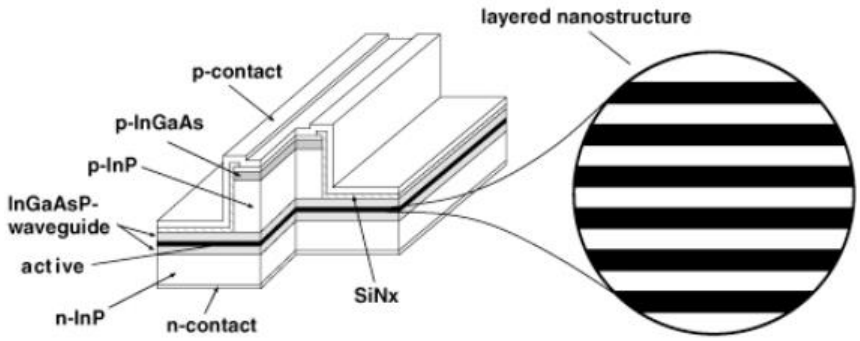

(b)

Figure 2.5: (a) Quantum well laser and (b) Multi-Quantum well laser. [30]

2.2 Photo Detectors

2.2.1 PN Photodiode

In PN photodiode, a depletion region is empty of free charge carriers consists of a large built-in electric field that opposes the movement of electrons from the n side to the p side and holes from p to the n. When the p-n junction is illuminated with light, electron-hole pairs are generated through absorption. Then due to a large built-in electric field in the depletion region, electrons and holes generated in a depletion region drifts to n and p sides, respectively. The flow of current is relative to the incident light energy [31].

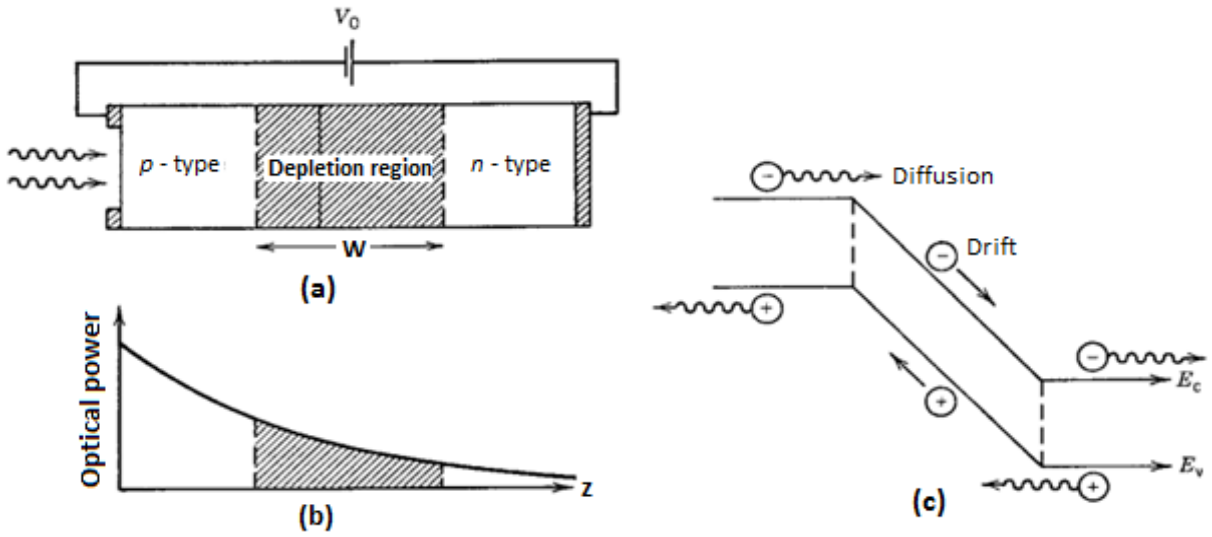

Figure 2.6: (a) p-n photodiode under reverse bias, (b) variation of optical power inside the photodiode, and (c) energy-band diagram . [31]

The transit time τ_{tr} of p-n junction photodiode can be written as [31]:

$$\tau_{tr} = W/v_d \tag{2.1}$$

Where *W is* the width of the depletion region, and v_d *is* drift velocity. *W* depends on the acceptor and donor concentrations, and v_d depends on the applied voltage and material used for the photo-diode.

The resistor and capacitor (*RC*) time constant τRC [31]:

$$\tau_{RC} = (R_L + R_S)C_P \tag{2.2}$$

Where R_L is the external load resistance and R_s is a series of resistance that arises from the resistance of the contacts, and the undepleted semiconductor material. C_p is the parasitic capacitance created due to junction and directly proportional to the diffused area and inversely proportional to the width of the depletion region.

2.2.2 PIN Photodiode

A simple way to raise the depletion-region width is by introducing a layer of undoped or lightly doped semiconductor material among the *p-n* junctions. The middle layer consists of nearly intrinsic material, and such a structure is referred to as a *PIN* photodiode. Because of its intrinsic nature, the mid-layer offers high resistance. As a result, most of the voltage drop happens across the middle layer. As a result, a large electric field occurs in the middle layer, and the depletion

region spreads throughout the *i* region; the depletion width *W* is controlled by changing the thickness of the central layer [31].

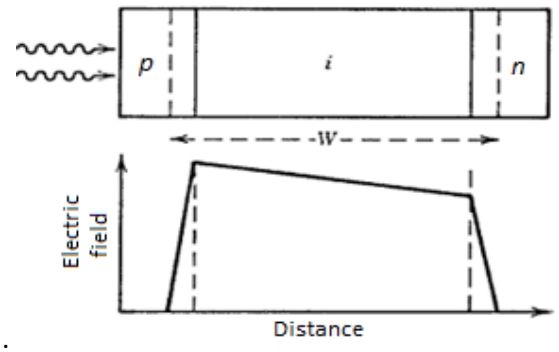

Figure 2.7: A p-i-n photodiode together with the electric-field distribution under reverse bias. [31]

2.2.3 Avalanche Photodiode (APD)

The phenomenon behind the internal current gain in *APD* is recognized as the impact ionization [32]. Under certain conditions, accelerating electrons acquire sufficient energy and give a part of its kinetic energy to other electrons in the valence band, and end up in the conduction band by leaving holes behind. The net outcome of impact ionization is the single primary electron produced through the absorption of a photon, which generates numerous secondary electrons and holes, all of which contribute to the photodiode current [33].

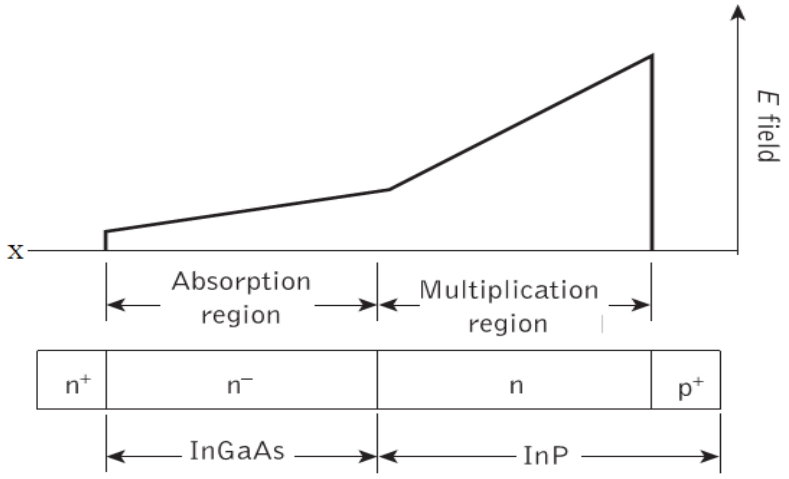

Figure 2.8: Separate absorption and multiplication (SAM) APD structure and electric-field distribution under reverse bias. [34]

Under reverse bias, a high electric field occurs in the InP n-p^+ junction and refers to the multiplication layer since secondary electron-hole pairs are generated here through impact ionization. The InGaAs n^+-n^- junction region is used as an absorption region in which most of

the incoming photons are absorbed and primary electron-hole pairs created. Electrons created in the absorption region cross the gain region and produce secondary electron-hole pairs liable for the current gain at the multiplication region [34].

2.3 Optical Fiber

Optical fibers made from glass or plastics materials and as thin as human hair and designed to guide light through their length. The optical fiber commonly has three coaxial regions. The innermost region is a light-guiding region known as the core, the middle section is cladding confines light into the core, and the outermost part is cover and shields cladding and core from abrasions, contamination, harmful influences of moisture, and so on. Optical fiber basically works based on total internal reflection. The light signal entered into fiber reflects from the sidewall and travels through the fiber length. A minor fraction of light can escape through sidewalls, but a majority reaches the other end of the fiber [35].

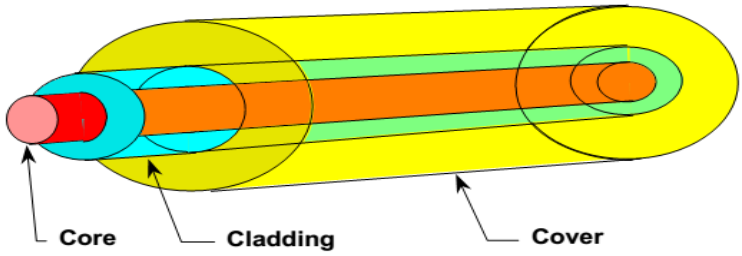

Figure 2.9: Optical fiber structure. [13]

The total internal reflection occurs when the rays of light striking a distance boundary separating an optically less dense medium and optically dense medium at a proper incident angle rather than passing through reflected [36].

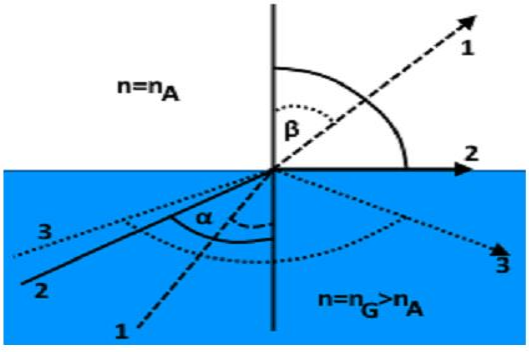

Figure 2.10: Total internal reflection. [10]

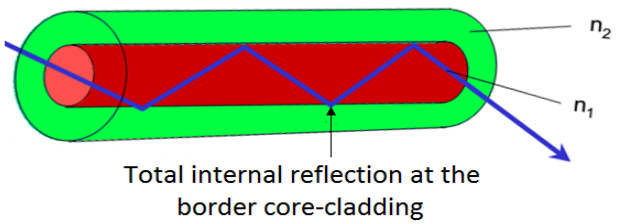

Figure 2.11: Total internal reflection in fiber. [13]

If the incident angle denoted by the symbol α and the angle of refraction as β, considering Snell's law of refraction as follows [10]:

$$\frac{sin\ \alpha}{\sin \beta} = \frac{n_A}{n_G} \tag{2.3}$$

Sinβ cannot be greater than one,

$$\sin \alpha_{critical} = \frac{n_A}{n_G} < 1 \tag{2.4}$$

Where, n is refractive index, n_A is air refractive index, n_G is glass refractive index, $n_1$is core refractive index, and n_2 is cladding refractive index.

2.3.1 Single Mode Step-Index Fiber

It has a significantly smaller core diameter than any other multimode fiber. The light that entered optical fiber either propagates through the core or reflected only a few times. All rays approximately follow equal time to travel the fiber length [37]. Figure 2.12 shows the optical signal propagating through single-mode step-index fiber, and n_1&n_2 are the refractive indexes of core and cladding.

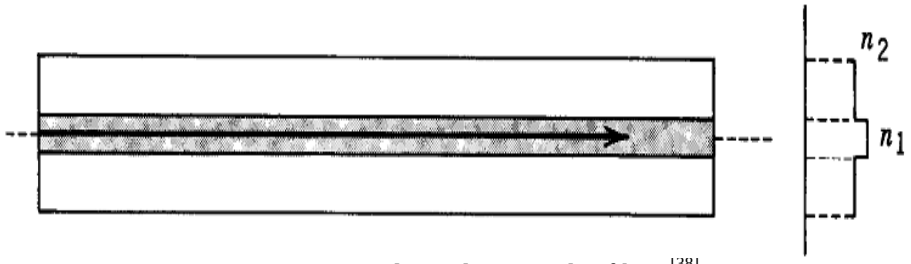

Figure 2.12: Single-mode step-index fiber. [38]

2.3.2 Multimode Step-Index Fiber

The refractive index of the core is constant all over and goes through a step change at the core-cladding boundary. Because of its bigger core size, more lights are coupled into this kind of optical fiber. However, there is typically more signal loss as well as more signal distortion because the light signal proceeds with multiple paths in the optical fiber [39]. Figure 2.13 shows the optical signal propagating through Multi-mode step-index fiber, and n_1&n_2 are refractive indexes of core and cladding.

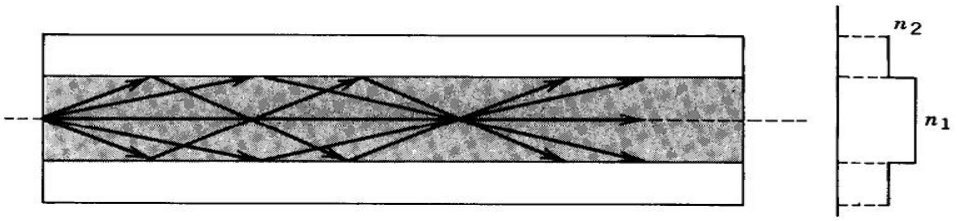

Figure 2.13: Multi-mode step-index fiber. [38]

2.3.3 Multimode Graded-Index Fiber

It is an improved multi-mode step-index fiber in terms of signal loss as well as signals distortion. The core refractive index of this fiber is constructed to change in a parabolic way and maximum at the core center [37]. Figure 2.14 shows the optical signal propagating through Multi-mode graded-index fiber. The n_1& n_2 are refractive indexes of core and cladding.

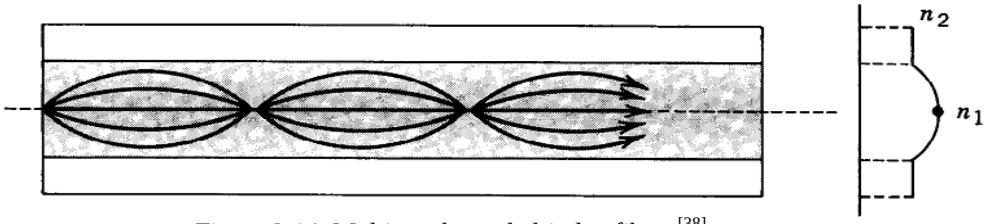

Figure 2.14: Multi-mode graded-index fiber. [38]

2.4 Channel Waveguides

The optical waveguides are made to confine light by fabricating specific waveguide structures on a layer of low refractive index material, such that light is guided through the process of total internal reflection [40]. The most common channel waveguides are buried waveguide, strip-loaded waveguide, ridge waveguide, rib waveguide, and diffuse waveguide [41]. Figure 2.15 shows different types of channel waveguides, and n is the refractive index, h height, d is thickness, w is width, x & y are the directions of optical confinement, and z is the direction of optical signal travel.

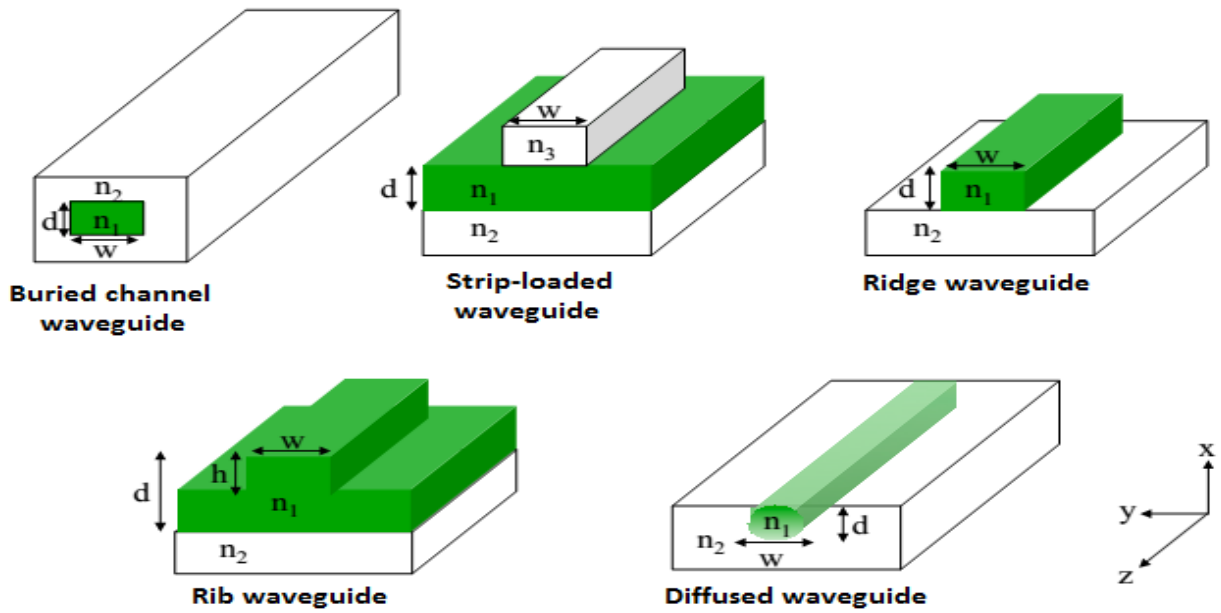

Figure 2.15: Channel waveguides. [41]

A buried channel waveguide is made with a high refractive index wave guiding core buried in a low-index surrounding medium, and its core can have any cross-sectional shape, and it is often a rectangular shape. A strip-loaded waveguide is made by loading a planar, which previously delivers optical confinement in the x-direction, with a dielectric strip of refractive index $n_3<n_1$ or a metal strip to facilitate optical confinement in the y-direction. The core of a strip waveguide is the n_1 section, with its thickness d resolute by the n_1 layer thickness and its width w demarcated by the width of the loading strip. A ridge waveguide has high optical confinement. The reason is surrounded by the three sides with low refractive index material (air). A rib waveguide contains a structure like a strip or a ridge waveguide, but the strip has the same index as the high index planar layer beneath and is a portion of the wave guiding core. A diffused waveguide is made by forming a high refractive index area in a substrate by diffusing dopants [41].

Chapter 3

Waveguides Loss and Magnetic Field Effect on Semiconductor Lasers and Photodiodes

3.1 Optical Fiber Losses

An optical signal propagating through a fiber gets continuously attenuated. The signal attenuation (α_{dB}) is the ratio of the optical output power (P_o) from fiber length *L* to the input power (P_i) and is expressed in decibel per kilometer dB/km [42].

$$\alpha_{dB} = \frac{10}{L} \log \frac{P_i}{P_o} \tag{3.1}$$

3.1.1 Dispersion

Dispersion is pulse expansion in optical fiber, and constituent such as numerical aperture, core diameter, refractive index, wavelength, and laser line-width in the optical fiber cause pulse broadening. The dispersion increases when fiber length increases and the total effects on the fiber optic system are known as Inter-symbol Interference (ISI) and happen when the pulse broadening due to dispersion makes the output pulses to overlap and become undetectable [43].

3.1.1.1 Material Dispersion

Light with unlike wavelength travels at different speeds in a medium; the long-wavelength waves travel faster than the short-wavelength waves. Consequently, a narrow pulse of light tends to expand as they travel down the optical fiber. The source spectral width determines the extent of material dispersion (D_m) [35]:

$$D_m = \frac{\lambda(\Delta\lambda)}{c} L \frac{d_n^2}{d\lambda^2} \tag{3.2}$$

Where, the peak wavelength ($\boldsymbol{\lambda}$), spectral width ($\Delta\boldsymbol{\lambda}$), the length of the core (*L*), and n is the refractive index of the core.

3.1.1.2 Waveguide Dispersion

The modes group velocities depend on wavelength, and the waveguide dispersion results from the dependence of filed distribution in optical fiber and the ratio between the core radius and wavelength (a/λ_o). If the ratio changed due to the altering, the relative portions of optical power in the core and cladding changed. Since the phase velocities in core and cladding are different,

the mode group velocity changed, and that causes waveguide dispersion [38].

3.1.1.3 Intermodal Dispersion

The pulse spreading as the result of this type of dispersion arises from the propagation delay variances among modes in multi-mode fiber. In this type of fiber, pulse with unlike modes travels at dissimilar group velocities across the channel. The pulse spreading is reliant on the slowest and fastest modes of transmission times [34].

3.1.1.4 Polarization Mode Dispersion

Optical fiber is basically modeled through two polarized orthogonal axes that named as principal state of polarization (PSP). The signal spreads in optical fiber divided into two components axes PSP; any polarization axis (fast and slow) spread at different speeds, and this is due to the difference in refractive indexes caused by inhomogeneous material [44].

Components of an optical pulse propagating at different speeds lead to spreading in making impulse for the optical receiver is insensitive to the polarization of light downward. The rate of expansion of impulses in time by polarization axis is known as the differential group delay (DGD), and it is an instant value that changes arbitrarily with fiber length and is measured in a picosecond. Polarization mode dispersion (PMD) is the rate of the linear average value of group delay to a wavelength λ and measured in picoseconds [44].

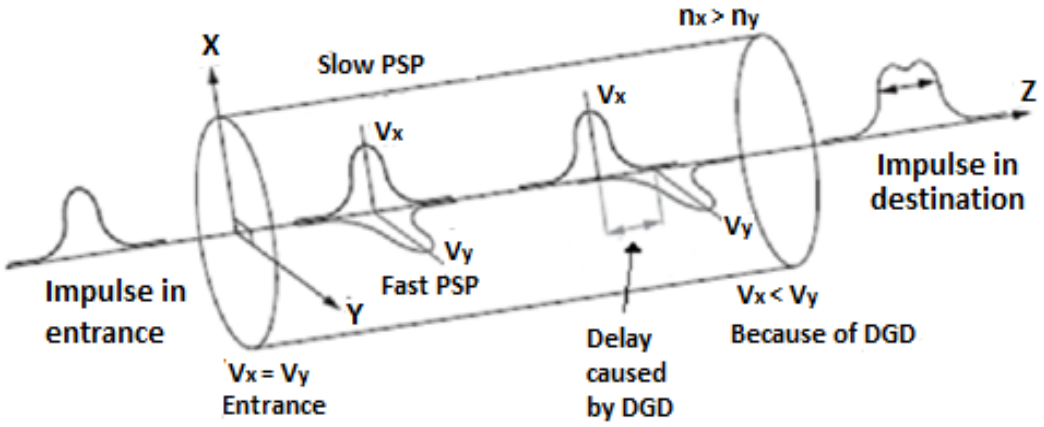

Figure 3.1: Polarization mode dispersion. [44]

3.1.2 Absorption Loss

Absorption is the process of transferring energy from the propagating light beam to the material structure and results in excitation in the charge carriers to a higher energy state [45].

3.1.2.1 Intrinsic Material Absorption Loss

This type of loss occurs from electronic absorption bands in the ultra-violate (UV) region and atomic vibration bands in the near-infrared (IR) region. The electromagnetic (EM) wave near infrared light forces ions to vibrate, and then certain energy is lost by being coupled into lattice vibrations (heat). Ultraviolet absorption happens when light interacts with an electron and give rise to a higher energy state [46].

3.1.2.2 Extrinsic Impurity Ions Absorption Loss

The extrinsic absorption happen due to the presence of impurities such as Fe, Cu, Co, Ni, Mn, and Cr absorb powerfully in the wavelength range 0.6-1.6μm. The main source of extrinsic absorption in state-of-the-art silica fibers is the occurrence of water vapors. A vibrational resonance of the OH^- occurs around 2.73μm. Its harmonic and mixture tones with silica produce absorption at the 1.39, 1.24, and 0.95μm wavelengths [31].

3.1.3 Scattering Losses

Scattering losses happen when a wave interacts with a particle in a route that removes energy in the way of propagation, and light just is directed into other directions [47].

3.1.3.1 Rayleigh Scattering Loss

Rayleigh scattering happens at arbitrary when there are small changes in the refractive index of materials in which the light signal travels. In this condition, it changes the refractive index of the core and cladding of the fiber optic cable. This loss occurred in a mini scale difference in the composition and density of the optical glass material itself, which is associated with the fiber manufacturing process. Rayleigh scattering accounts for around 96% of attenuation in optical fiber [47].

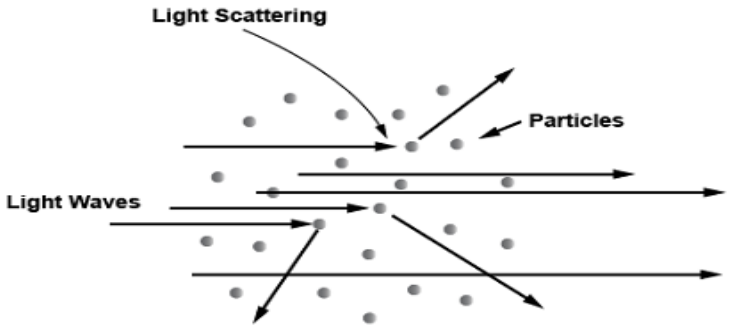

Figure 3.2: Rayleigh scattering. [47]

It is the scattering of light by particles that are much smaller in size than the light wavelength. The Rayleigh scattered radiation raises quickly as the ratio of particle size to wavelength increases and proportional to λ^{-4} and decreases rapidly with an increase in wavelength. This type of scattering model is not used when the size of particles higher 10% of incident radiation wavelength. In this circumstance, Mie's scattering model is used to determine the scattered radiation [47].

The Rayleigh scattering loss expression in dB/km and approximated as follows [36]:

$$L = 1.7\left(\frac{0.85}{\lambda}\right)^4 \tag{3.3}$$

Where, L is the Rayleigh scattering loss, and λ is the wavelength.

3.1.3.2 Mie Scattering Loss

It is the scattering of light by the particles, which are 10% bigger than the light wavelengths. Mie scattering happens due to inhomogeneity, such as core-cladding refractive index variation over fiber length, impurities at the core-cladding boundary, and diameter variations [48].

3.1.3.3 Brillouin Scattering Loss

This sort of scattering occurs because of the nonlinearity of a medium and causes a modulation of light by the thermal molecular vibrations fiber. The scattered light exists as upper and lower sidebands and separates from the light entered by the modulation frequency. The incident photon generates phonon of acoustic frequency and scattered photon. The combination of optical fields and acoustic waves happens via electrostriction in this type of scattering [49]. It causes an optical frequency shift. This type of scattering is only important above threshold power density [42].

3.1.3.4 Raman Scattering Loss

This type of scattering is a nonlinear scattering, and it can severely limit the performance of a multichannel field, and its frequency is shifted down. Near the right end, a significant part of the power shifted into longer-wavelength components by stimulated Raman scattering. The incident light generates the frequency-shifted radiation called Stokes waves [50].

3.1.4 Bending Loss

3.1.4.1 Macro Bending Loss

The radiation losses occur at the bending of optical fibers; when the energy in the evanescent

field at the bending exceeds the velocity of light in the cladding, the guidance mechanism is inhibited, and the light energy is discharged from the fiber. The portion of the mode on the exterior of bending is essential to travel faster than on the inside. So, a wave front perpendicular to the direction of propagation is maintained, as shown in figure 3.3. Hence, the portion of the model in the cladding needs to travel quicker than the velocity of light in that medium, and this is not likely the energy associated with this portion of the mode lost through radiation [34].

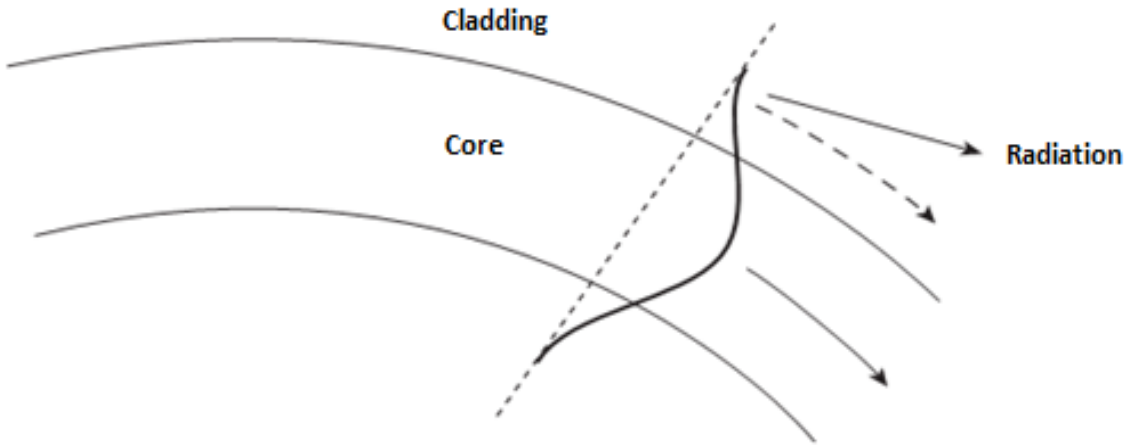

Figure 3.3: Fiber bending loss. [34]

The loss can generally be represented by a radiation attenuation coefficient (α_r) [51].

$$\alpha_r = c_1 e^{-c_2 R} \tag{3.4}$$

Where R is the radius of curvature of the fiber bend and c_1 & c_2 are constants which are independent of R.

Furthermore, large bending losses occur in multimode fibers at a critical radius of curvatures Rc [52].

$$R_c \sim \frac{3n_1^2\lambda}{4\pi(n_1^2-n_2^2)^{\frac{3}{2}}} \tag{3.5}$$

Where λ is operating wavelength, $n_1$is core refractive index, and $n_1$is cladding refractive index.

The critical radius of curvature for a single-mode fiber R_{cs} can be estimated as [53].

$$R_{cs} \sim \frac{20\lambda}{(n_1-n_2)^{\frac{3}{2}}}\left(2.748 - 0.996\frac{\lambda}{\lambda_c}\right)^{-3} \tag{3.6}$$

Where, λ_c is the cutoff wavelength for the single-mode fiber, λ is operating wavelength, $n_1$is core refractive index, and $n_1$is cladding refractive index.

3.1.4.2 Micro Bending Loss

A micro bend is a microscopic curving, crack, or irregularity in the cladding and core of an optical fiber cable line that induces small distortions ultimately causes signal attenuation and foster power losses in the optical fiber [54].

3.1.5 Return Loss

It is the loss of the light signal and happens when light is reflected off the connector and travels back to the light source along with fiber. This phenomenon is known as Fresnel reflection. It also happens when there are changes in the refractive index of materials in which the light travels, such as fiber core and the air gap between fibers interconnection [55].

3.2 Silicon on Insulator (SOI) Waveguides Loss

Light propagating through waveguides experiences several types of loss. Some of them are related to the media itself, technological processes, and some imperfections. Equation 3.7 shows different types of losses that occur in the Silicon on Insulator (SOI) waveguides [56].

$$L_{tot} = L_a + L_{ss} + L_{vs} + L_{cs} \tag{3.7}$$

L_{tot} is a total straight waveguide loss, expressed in dB/cm. L_a is a material absorption loss that is wavelength dependent and increases based on silicon doping [57]. L_{ss} is the interface-induced scattering, and it depends on the field propagating in the material. The scattering amount is relative to E_S^2 (n_2^2 - n_1^2), mainly the intensity of the electromagnetic field on a waveguide surface and the difference between squared refractive indexes of waveguide core and cladding [58]. It also depends on the roughness of the waveguide surface associated with sidewall etches, interfaces between Si and SiO_2 [59]. L_{vs} is related to volumetric variations of the refractive index and intrinsic in the process of wafer manufacturing since implanting and growth have the potential of producing islands of impurities and crystals defects. L_{cs} is the type of loss caused because of the coupling of propagating modes with substrate modes [58]. An additional source of loss is bending loss and the mode-mismatch between a mode in the straight waveguide and bend. This mismatching causes reflection at the interfaces between straight and bent waveguides and results in power dissipation; the effect is more intense for small curvature bends [60].

3.3 Magnetic Field Effect on Semiconductor Lasers

Many types of researches have done show that the external magnetic field influences the performances of lasers. The effects depend on the laser types, the strength of the magnetic field, the field direction, and temperature.

3.3.1 Magnetic Field Effect on VCSEL at Room Temperature

When the magnetic field is applied in the direction ***B//n*** (field and current flow the same direction) to the VCSEL, Lorentz force alters the flow of the outward-bound current. Subsequently reduces the diffusing current. So, carrier density increases, and that causes an increase in intensity, higher side shifts in oscillation frequency, and lower side shifts in wavelength. Figure 3.4 shows the overhead outlook of the laser and its current flow in the ***B//n*** direction [18].

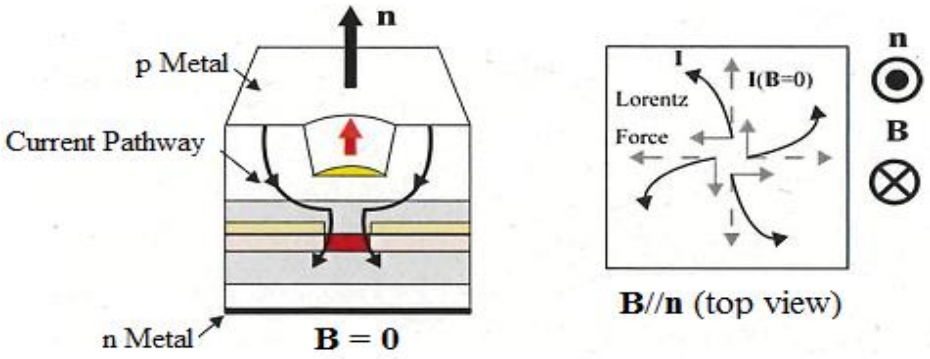

Figure 3.4: Change in current flow by Lorentz force B//n top view. [18]

3.3.2 The Influence of Magnetic Field on Multi Quantum Well Laser

A Quantum Well is formed when well material which has a lower band gap inserted between two barrier materials with a higher band gap provided the thickness *L* of well materials less than the de-Broglie wavelength [29]. In quantum well, the charge carriers can no longer move freely in three dimensions but two dimensions. The electrons in the third direction are bound to a state with a characteristic wave function and energy. Only a discrete set of such a bound state exists as given in the following equations [29], [61]:

$$E(n, k_x, k_y) = (\hbar^2/2m_n^*)(k_x^2 + k_y^2) + E_n \tag{3.8}$$

$$E_n = \hbar^2/2\, m_n^*(n\pi/L_z)^2 \tag{3.9}$$

Where E_n is the n^{th} confined-particle energy level for carrier motion normal to well and m_n^* is the

effective mass of the carrier in the level n, L_z is the thickness of well material, k_x & k_y are wave vectors in x and y-direction $\hbar = h/2\pi$ is called a modified Planck's constant.

3.3.2.1 Landau Effect

In the MQW laser, the strong magnetic field oriented perpendicular to charged particles causes to create a ladder of Landau levels connected to each sub-band [62]. As a result, inter sub-band Landau resonances arise proportional to the field strength. The Landau levels of each sub-band line up with a corresponding Landau level at the different sub-band, producing a level index-change δ_n = 1, 2, 3--- [62].

$$E_{trans} = \delta_n \,.\, \hbar\omega_c \tag{3.10}$$

Where, E_{trans} is the inter sub-band transition energy, $\omega_c = qB/m^*$, is the cyclotron frequency, q is charge, m^* is effective mass, and B is magnetic field.

The Landau effect causes a frequency shift to a higher frequency side on MQW laser output [20]. The necessary condition for the formation of Landau levels is $KT << \hbar\omega_c$, where ω_c is the angular frequency of the cyclotron orbit. This condition is achieved at low temperatures (T<100K) and strong magnetic fields and around the room temperature; the thermal agitation is high enough to wash out Landau splitting [20].

3.3.2.2 Effects on Recombination Rate of Charge Carriers

In semiconductor structures, the band-to-band optical transition obeys the k-selection rule [63]. The electron-hole recombination process obeys momentum conservation; both charge carriers possessing identical wave-vectors can recombine to produce a photon. When the static magnetic field is applied perpendicular to the QW planes (***B//n***), the charge carriers traveling along the injection current direction remain unaffected. But the charge carriers that diffuse out of the injection current as a result of thermal agitation having a component of momentum in the direction normal to the magnetic field direction (parallel to the QW planes) experience magnetic confinement. The cyclotron frequencies ($\omega_c = Bq/m^*$) for electrons and holes that had the same momentum differ due to the difference in the effective masses (m^*) and charges (q). As a consequence, the output optical power decreases while the magnetic field increases [20]. Around room temperature and low magnetic field values, the gain of the MQW laser shifted to the lower frequency side [64]. The magnetic field sweeps away some of the diffusing charges carriers from recombining in the quantum wells even though they are confined magnetically and quantum

mechanically. It leads to a reduction in the band filling of the lasing state of the QW laser and changes in the oscillating wavelength of the MQW laser towards the lower frequency side. But when the field is applied parallel to QW planes ($\boldsymbol{B \perp n}$), it pushes a small number of charge carriers out of the well related to the strength of quantum confinement and Lorentz force [20].

3.4 Magnetic Field Effect on Silicon Photodiodes

The main function of photodiodes is converting an optical signal to an electrical signal. During its operation, when a photodiode subjected to the light, the net output current [65]:

$$I = I_o\,(e^{\frac{eV}{kT}} - 1) - I_L \tag{3.11}$$

Where V is applied voltage, I_o is reverse saturation current, k_B is Boltzmann constant, T is absolute temperature, and I_L is the light current.

According to the laws of statistical physics, the current is related to the energy E gained by the free carriers [22].

$$I = I_o\,(e^{\frac{E}{kT}} - 1) + I_L \tag{3.12}$$

When a magnetic field of flux density *B* affects the electron of velocity *v* is given by:

$$E = BevL + eV$$

Thus:

$$I = I_o\,(e^{\frac{BevL+eV}{kT}} - 1) + I_L \tag{3.13}$$

When the magnetic field and the potential are weak [64]:

$$x = \frac{BevL+eV}{kT} \ll 1 \tag{3.14}$$

In this case:

$$I = I_o\left(\frac{BevL+eV}{kT}\right) + I_L \tag{3.15}$$

When the silicon photodiodes are subjected to the magnetic field, the charge carriers gain energy, and both dark current and light current rise depending on magnetic field strength [22]. The dark current is the output current produced without optical radiation to the photodiode. The light current is generated when the photodiodes illuminate to optical radiation.

Chapter 4

Methodology

4.1 Description about Experimentation

This thesis experimentation mainly focused on two scenarios. The first scenario is concerned with the influence of change in input signal frequency to magnetic field effect on output signal when laser and photodiode concurrently as well as separately exposed to the magnetic field. The second scenario is concerned with the effect on the output signal when both laser and photodiode are concurrently exposed to the magnetic field and how the effect differs comparatively from each transducer separately subjected to the magnetic field. Finally, the effects considered in each scenario were analyzed by comparing the results measured from all experiments.

First Experiment:

The first experiment was organized to identify the effect on the output signal when a laser is subjected to a magnetic field oriented ***B//n*** and how the magnetic field effect on the output signal differs when the frequency varies. In this experiment, the optical signal outputted from VCSEL was reflected by the mirror and coupled to a PIN photodiode. During experimentation, the VCSEL was exposed to a static magnetic field at 0T, 400mT, 600mT, 800mT, and 1000mT, and then the output voltage was measured and recorded at 3 kHz and 10 kHz.

Second Experiment:

The second experiment was prepared to detect the effects on the output signal when a photodiode is subjected to the magnetic field oriented ***B//n*** and how the magnetic field effect changes when the frequency varies. The same as experiment one, in this experiment, the optical signal outputted from VCSEL reflected by a mirror and coupled to PIN photodiode. Then PIN photodiode was subjected to the static magnetic field at 0T, 400mT, 600mT, 800mT, and 1000mT, and then output voltage was measured and recorded at 3 kHz and 10 kHz.

Third Experiment:

The third experiment was organized to identify the effect on the output signal when both transducers (laser and photodiode) are simultaneously subjected to the magnetic field oriented ***B//n*** and the change in magnetic field effect on the output signal when the frequency changes. Likewise experiment-1 and 2, in this experiment, the optical signal outputted from

VCSEL is reflected by the mirror and coupled to the PIN photodiode. During experimentation, both VCSEL and PIN photodiode were concurrently exposed to the static magnetic field at 0T, 400mT, 600mT, 800mT, and 1000mT. Then output voltage was measured and recorded at 3 kHz and 10 kHz.

Fourth Experiment:

The fourth experiment was prepared to identify the effect on the output signal when a laser is subjected to a magnetic field oriented $\boldsymbol{B \perp n}$ and how the magnetic field effect on the output signal differs when the frequency varies. In this experiment, the optical signal outputted from VCSEL was directly coupled to the PIN photodiode. During experimentation, the VCSEL was subjected to a static magnetic field at 0T, 400mT, 600mT, 800mT, and 1000mT, and then output voltage was measured and recorded at 3 kHz and 10 kHz.

Fifth Experiment:

The fifth experiment was organized to detect the effects on the output signal when a photodiode is subjected to the magnetic field oriented $\boldsymbol{B \perp n}$ and how the effect changes when the frequency varies. In this experiment, the optical signal outputted from VCSEL was directly coupled to the PIN photodiode. Then PIN photodiode was subjected to the static magnetic field at 0T, 400mT, 600mT, 800mT, and 1000mT, and output voltage was measured and recorded at 3 kHz and 10 kHz.

4.2 Materials and Experimental Setup Arrangement

Initially, all the necessary materials for the experimental setup were collected. The VCSEL (850 nm) and PIN photodiode were collected from Ethio-Telecom. The standard laser's protective cover consists of ferromagnetic material [20]. So, the VCSEL's and PIN photodiode's covers were removed for experimentation. The electromagnet was constructed in the laboratory generates up to 1000mT at 20A with proper clearance between two poles to insert VCSEL and PIN photodiode in both $\boldsymbol{B//n}$ and $\boldsymbol{B \perp n}$ alignment. All the other materials were collected from the advanced optics laboratory where the experiments were conducted. Even though the magnetic field effect differs based on transducers type [18] - [22], in this experimental setup, only VCSEL & PIN photodiode were able to find and used.

4.2.1 Transmitter

The transmitter part contains 3.36V & 5V DC power supply, a laser driver circuit, and VCSEL

(850nm). The laser driver circuit was constructed using NE555 timer, field-effect transistor (FET), resistors, variable resistor, and capacitors, as shown in figure 4.1 below. The laser driver was connected to 5 VDC, and VCSEL connected to a 3.36 VDC power supply. Then laser driver produced a square wave signal with a frequency range from 3 kHz to 10 kHz. The frequency was adjusted using the variable resistor in the circuit. During experimentation, the VCSEL supplied an 8.5 mA input current at 3 kHz and 10mA at 10 kHz from the source.

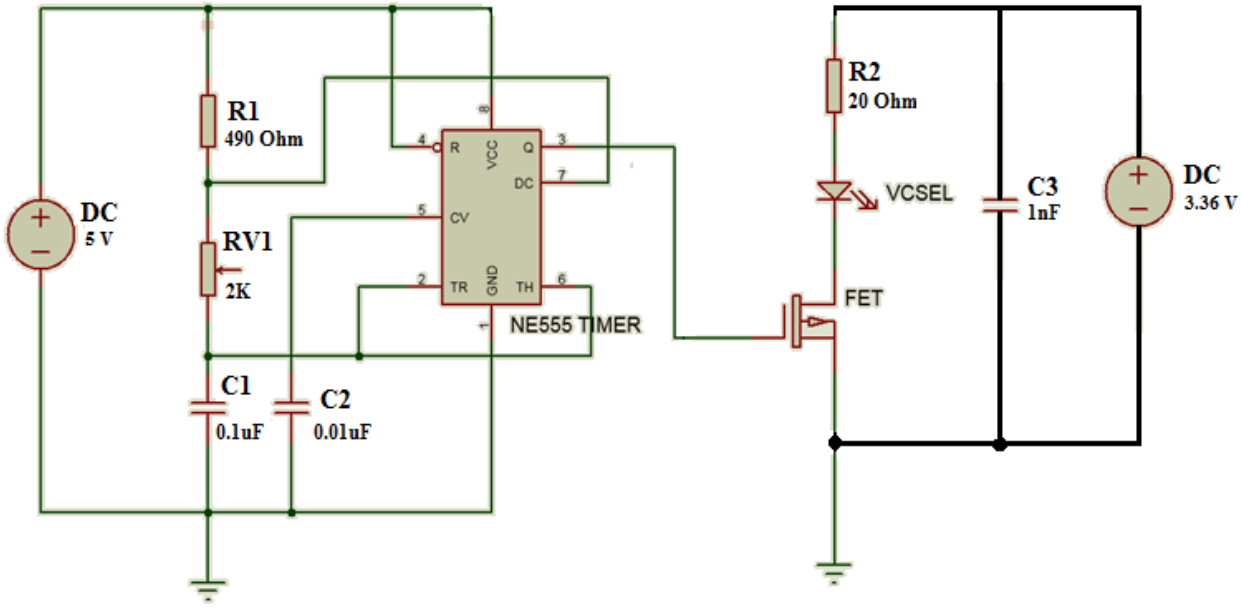

Figure 4.1: Laser driver circuit.

4.2.2 Receiver

The receiver part contains 3.36V DC, 10kΩ resistor, and PIN photodiode. The cathode of PIN photodiode connected to 3.36 V DC and anode to 10kΩ resistor. The photocurrent produced by PIN photodiode flowed through a 10kΩ resistor and converted to voltage for measurement. Then output voltage was measured across a 10kΩ resistor using both multi-meter and oscilloscope as shown in figure 4.2 below.

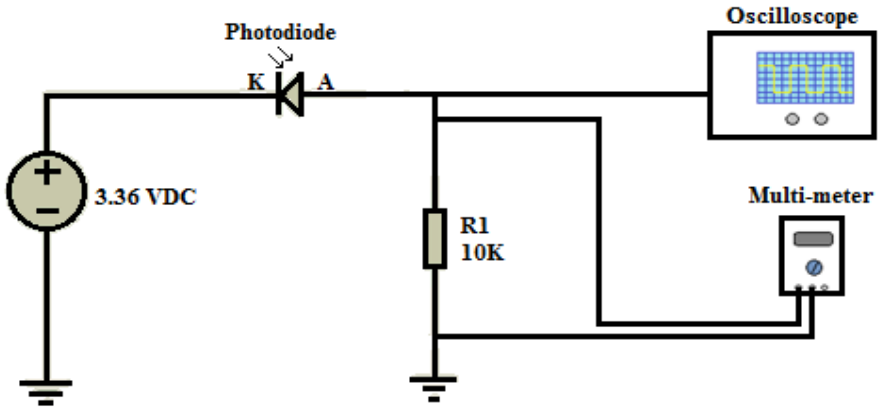

Figure 4.2: Receiver circuit.

4.2.3 Mirror

During the experimentation, for ***B//n*** alignment, the optical signal outputted from VCSEL was coupled to a PIN photodiode using a mirror.

4.2.4 Electromagnet

For magnetic field generation, we have constructed an electromagnet that was capable of generating 1000mT. In doing so, initially, two pieces of iron rods used as a core in the electromagnet were prepared in suitable size and shape using a lathe machine. After that, insulating materials were placed over both irons, and then 2.5mm^2 copper wire was wound over them, as shown in figure 4.3. Once the coiling was completed, then all the necessary testing was carried out. Then electric power supplied to the electromagnet to measure the maximum magnetic field can be produced with 20A available power supply in the lab. The electromagnet produced up to 1000mT at 20A, with a suitable range of clearance between two iron rods (poles) to insert laser and photodiode for ***B//n*** and ***B⊥n*** alignment to conduct experiments.

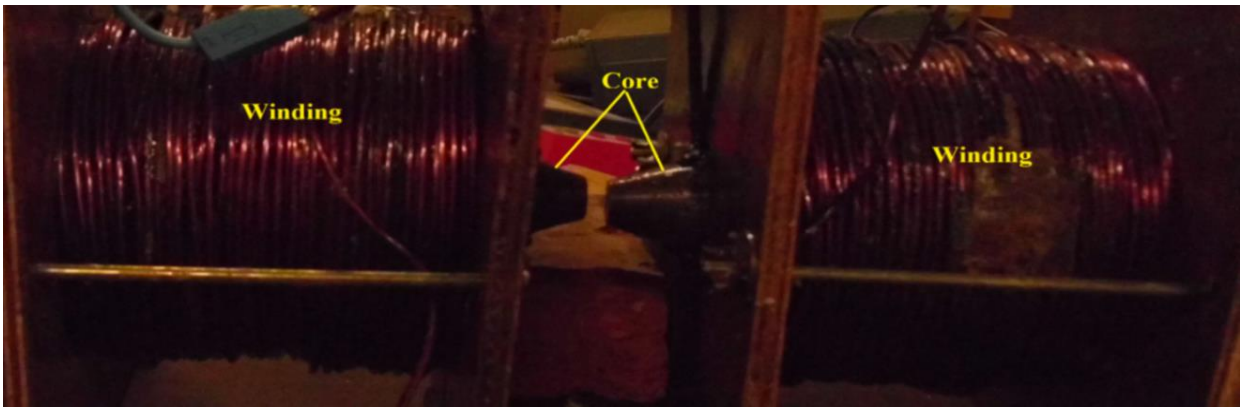

Figure 4.3: Electromagnet

4.2.5 Magnetic Field Alignment with VCSEL and PIN Photodiode

The following figure 4.4 & 4.5 show the magnetic field orientation. The symbols ***B*** represented magnetic flux density and ***n*** the normal direction of VCSEL's and PIN photodiode's layered surface area [19]. The magnetic field oriented perpendicular to VCSEL's & PIN photodiode's layered surface represented as ***B//n*** and parallel to VCSEL's & PIN photodiode's layered surface denoted as $\boldsymbol{B}^{\perp}\boldsymbol{n}$.

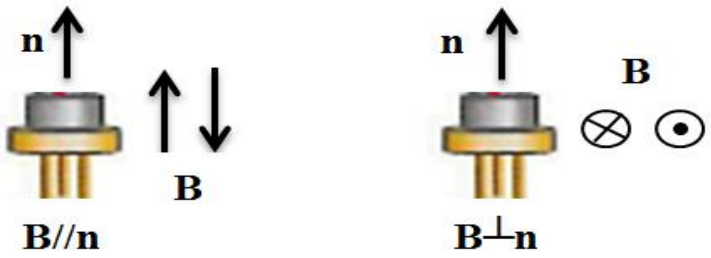

Figure 4.4: The direction of magnetic field orientation with VCSEL.

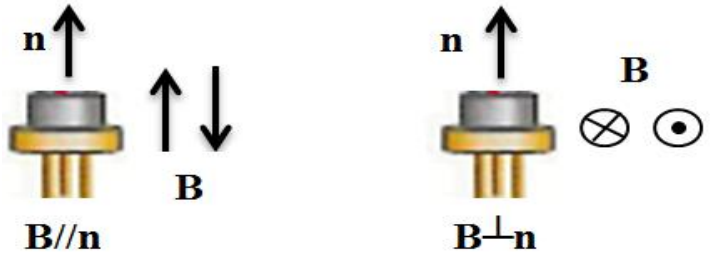

Figure 4.5: The direction of magnetic field orientation with PIN Photodiode.

4.2.6 Complete Experimental Setup

Generally, under this experimental setup arrangement, five experiments were conducted. Materials and components used in whole experiments were the same except for ***B//n*** alignment in the first three consecutive experiments mirror was used to couple the VCSEL output to PIN photodiode. Rather than that experimental setup arrangement remained the same for all experiments during the whole experimentation.

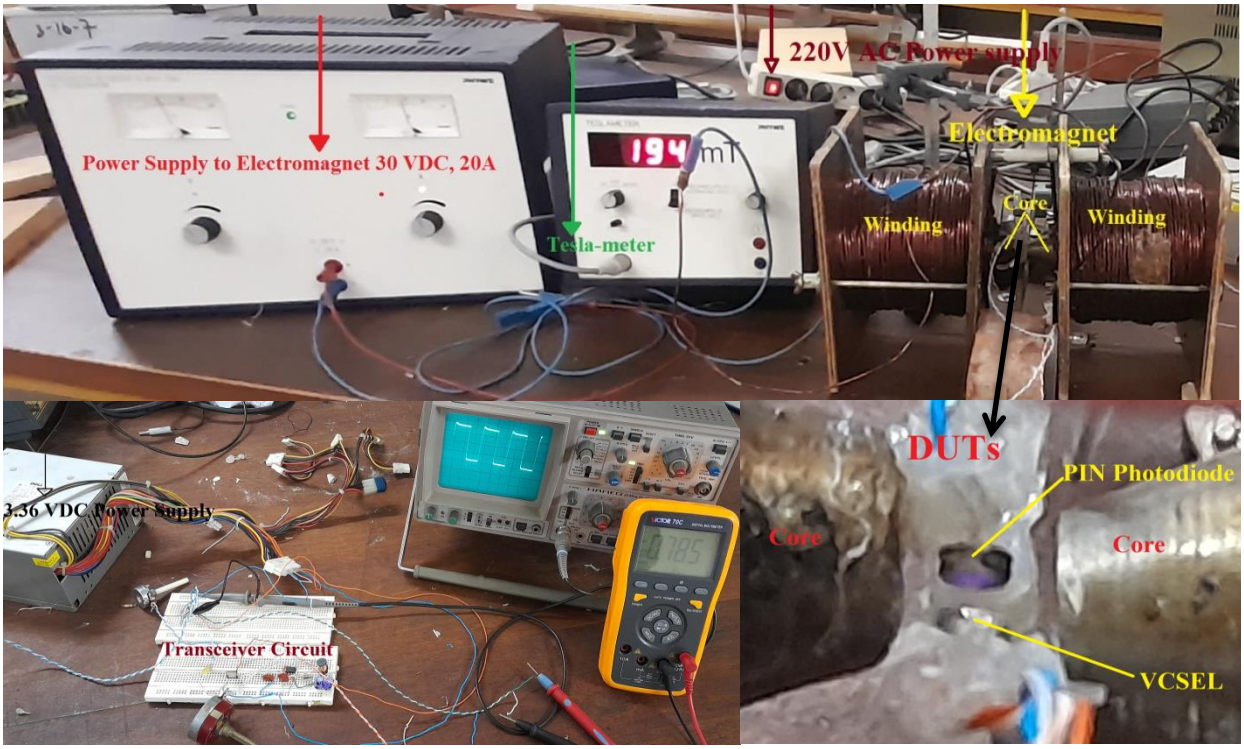

Figure 4.6: Full experimental setup.

The setup shown in the above fig.4.6 contains the transmitter and receiver parts. The laser driver circuit in the transmitter was connected to 5V DC and VCSEL to a 3.36V DC power supply. Then laser driver produced a square wave signal with an intended frequency of 3 kHz and 10 kHz, and then VCSEL converted it to an optical signal equivalent to an electrical square wave signal. For ***B//n*** alignment, the optical signal outputted from VCSEL was reflected by the mirror and coupled to the PIN photodiode. But, for $\boldsymbol{B \perp n}$ orientation, the optical signal outputted from VCSEL was directly coupled to a PIN photodiode. At the receiver, the PIN photodiode converted the optical signal to an electrical signal. Then the photocurrent from the PIN photodiode was converted to a voltage by the 10 KΩ resistor for measurement. The electromagnet is generated a maximum static magnetic field up to 1000mT at 20A with proper clearance between two poles to insert laser and photodiode in both ***B//n*** & $\boldsymbol{B \perp n}$ alignment. The magnetic field strength was controlled by adjusting the magnitude of the electric current supplied to the electromagnet between 0 to 20A. Then VCSEL and PIN photodiode were separately and concurrently exposed to magnetic field oriented ***B//n*** & $\boldsymbol{B \perp n}$, at 3 kHz and 10 kHz, around room temperature (20 ^{0}C). Finally, the output voltage was measured and recorded at different magnetic flux densities and frequencies using an oscilloscope and multi-meter at the receiver across a 10kΩ resistor.

4.3 Measurement

For output voltage measurement, in experiment-1, VCSEL was exposed to the static magnetic field oriented ***B//n***. Once the measurement was completed with the first experiment, experiment-2 was conducted by exposing the PIN photodiode to the static magnetic field oriented ***B//n*** and output voltage measured. In the third experiment, both VCSEL and PIN photodiode was concurrently exposed to the static magnetic field oriented ***B//n***. Then output voltage was measured. In the fourth and fifth experiments, both VCSEL and PIN photodiode were separately subjected to the static magnetic field oriented ***B⊥n*** and output voltage measured.

All experiments were conducted at around room temperature. Then the output voltage is measured and recorded at 0, 400, 600, 800, and 1000mT at both 3 kHz and 10 kHz.

Experiment -1

Procedures:

- ✓ Set input voltage first and supplied to laser driver circuit and VCSEL.
- ✓ Coupled VCSEL outputted optical signal to PIN photodiode using mirror.
- ✓ Adjusted the magnetic field strength by varying the magnitude of electric current supplied to electromagnet.
- ✓ VCSEL exposed to the static magnetic field oriented ***B//n*** at 0, 400, 600, 800, and 1000mT.
- ✓ Output voltage and current measured and recorded at 3 kHz & 10 kHz.

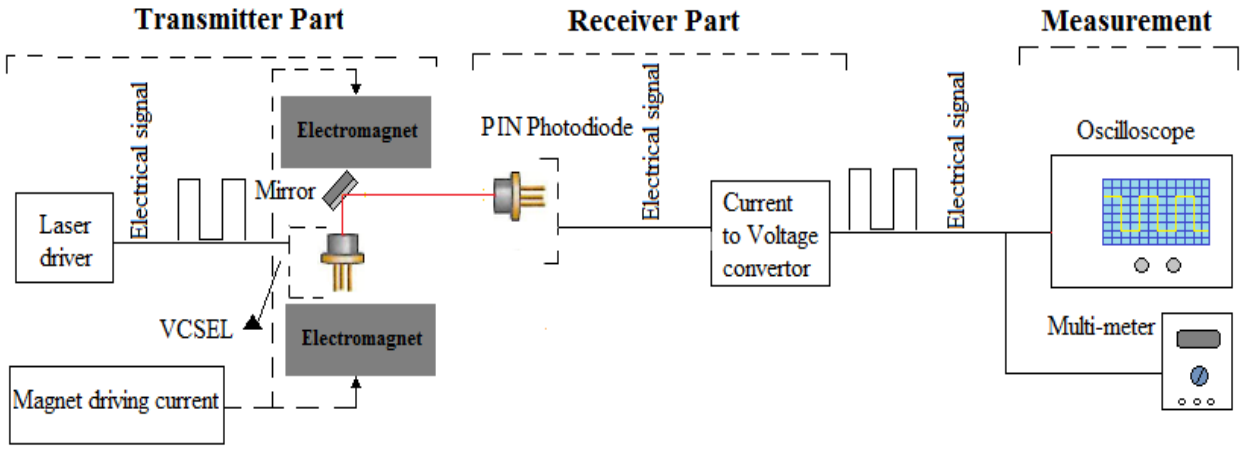

Figure 4.7: Output voltage measurement when only VCSEL exposed to magnetic field oriented ***B//n***.

.

Experiment -2

Procedures:

- ✓ Set input voltage first and then supplied to laser driver circuit and VCSEL.
- ✓ Coupled VCSEL outputted optical signal to PIN photodiode using mirror.
- ✓ Adjusted the magnetic field strength by varying the magnitude of electric current supplied to electromagnet.
- ✓ PIN photodiode exposed to the static magnetic field oriented ***B//n*** 0, 400, 600, 800, and 1000mT.
- ✓ Output voltage and current measured and recorded at 3 kHz & 10 kHz.

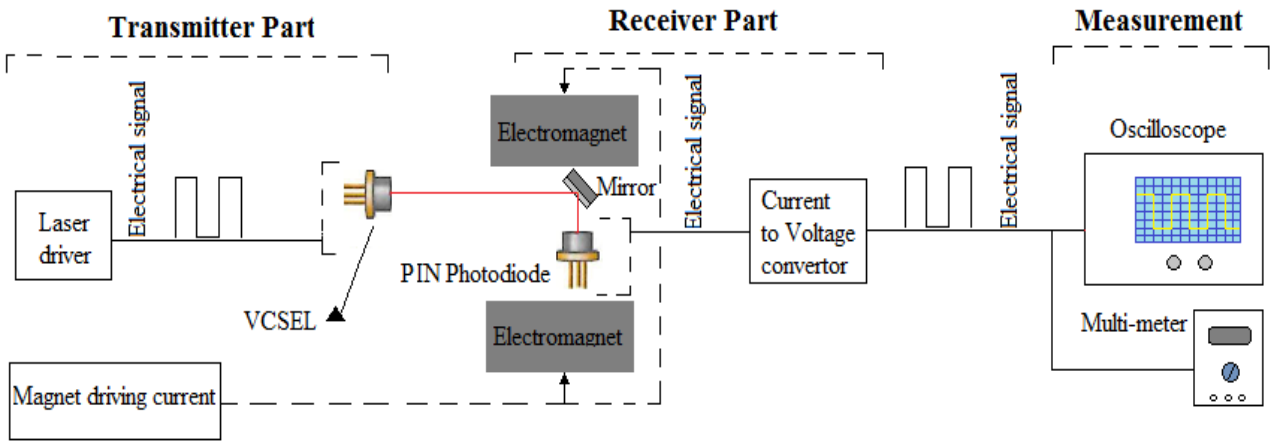

Figure 4.8: Output voltage measurement when only PIN photodiode exposed to magnetic field oriented ***B//n***.

Experiment -3

Procedures:

- ✓ Set input voltage first and then supplied to laser driver circuit and VCSEL.
- ✓ Coupled VCSEL outputted optical signal to PIN photodiode using mirror.
- ✓ Adjusted the magnetic field strength by varying the magnitude of electric current supplied to electromagnet.
- ✓ Both VCSEL and PIN photodiode concurrently exposed to the static magnetic field oriented ***B//n*** at 0, 400, 600, 800, and 1000mT.
- ✓ Output voltage and current measured and recorded at 3 kHz & 10 kHz.

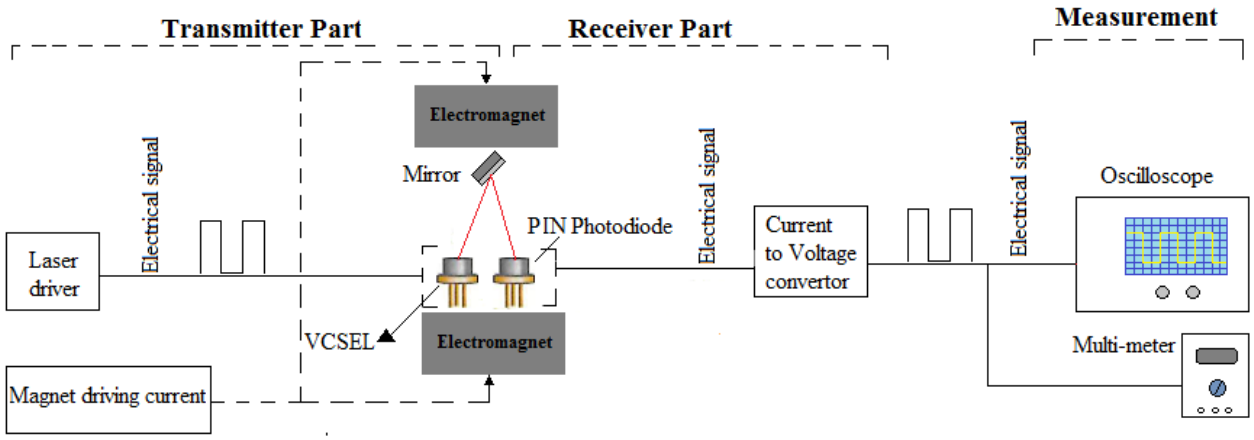

Figure 4.9: Output voltage measurement when both VCSEL and PIN photodiode concurrently exposed to the magnetic field oriented ***B//n***.

Experiment -4

Procedures:

- ✓ Set input voltage first and supplied to laser driver circuit and VCSEL.
- ✓ Directly coupled VCSEL outputted optical signal to PIN photodiode.
- ✓ Adjusted the magnetic field strength by varying the magnitude of electric current supplied to electromagnet.
- ✓ VCSEL exposed to the static magnetic field oriented $\boldsymbol{B \perp n}$ at 0, 400, 600, 800, and 1000mT.
- ✓ Output voltage and current measured and recorded at 3 kHz & 10 kHz.

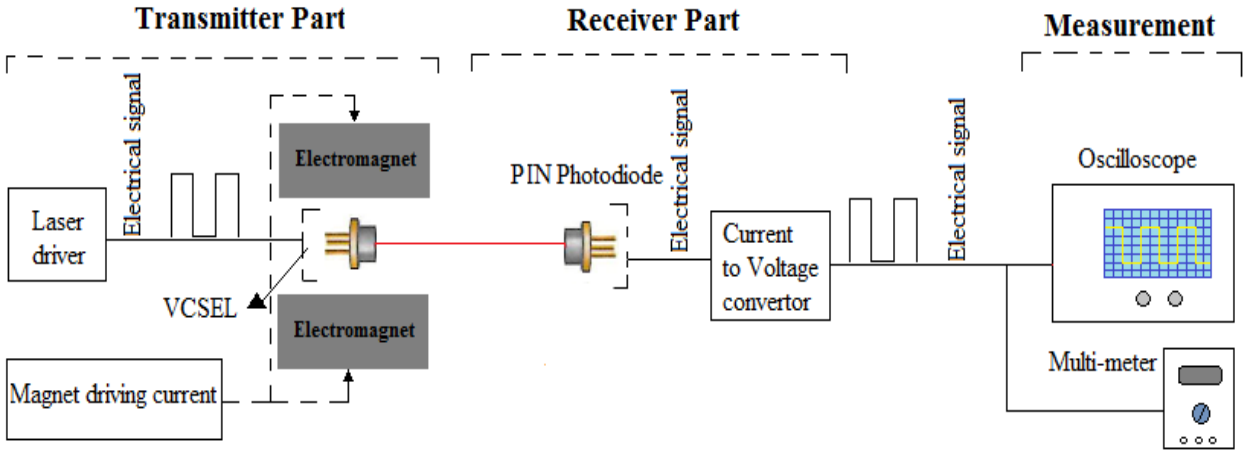

Figure 4.10: Output voltage measurement when only VCSEL exposed to magnetic field oriented $\boldsymbol{B \perp n}$.

.

Experiment -5

Procedures:

- ✓ Set input voltage first and supplied to laser driver circuit and VCSEL.
- ✓ Directly coupled VCSEL outputted optical signal to PIN photodiode.
- ✓ Adjusted the magnetic field strength by varying the magnitude of electric current supplied to electromagnet.
- ✓ PIN Photodiode exposed to the static magnetic field oriented $\boldsymbol{B}^{\perp}\boldsymbol{n}$ at 0, 400, 600, 800, and 1000mT.
- ✓ Output voltage and current measured and recorded at 3 kHz & 10 kHz.

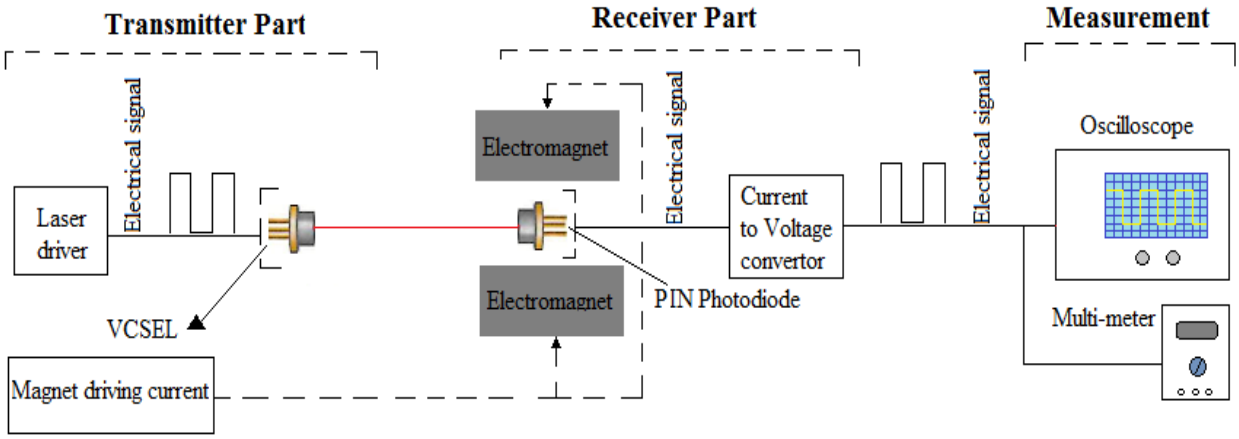

Figure 4.11: Output voltage measurement when only PIN photodiode exposed to magnetic field oriented $\boldsymbol{B}^{\perp}\boldsymbol{n}$.

Chapter 5

Results and Discussion

To study the effects on the output signal, totally five experiments were conducted. During experimentation, input voltage and current were supplied to VCSEL, as shown in fig.4.6. Then at the receiver, the photocurrent from PIN photodiode converted to a voltage by 10KΩ resistor and measured at 0, 400, 600, 800, & 1000mT of the magnetic field applied to VCSEL and PIN photodiode oriented ***B//n*** & ***B⊥n*** at 3 kHz and 10 kHz as shown in the following tables. The V_L and V_P denoted output voltage measured when VCSEL and PIN photodiode individually exposed to the static magnetic field oriented ***B//n*** & ***B⊥n*** at 3 kHz and 10 kHz. The V_{LP} represented output voltage measured when both VCSEL and PIN photodiode concurrently exposed to the static magnetic field oriented ***B//n*** at 3 kHz and 10 kHz.

5.1 Output Voltage Measured

Initially, the VCSEL was exposed to the static magnetic field oriented ***B//n*** & ***B⊥n*** at 3 kHz and 10 kHz, and then output voltage was measured from the experimental setup and recorded. The following table 5.1 and 5.2 show the output voltage measured at different magnetic flux densities and frequencies.

Table 5.1: Output Voltage measured when VCSEL exposed to the static magnetic field @ 3 kHz.

V_{IN} (V)	I_{IN}(mA)	Magnetic Flux Density (mT)	V_L (mV) for *B//n*	V_L (mV) for *B⊥n*
3.36	8.45	0	44	62
3.36	8.45	400	45	62
3.36	8.45	600	46	62
3.36	8.45	800	47	62
3.36	8.45	1000	47	62

Table 5.2: Output Voltage measured when VCSEL exposed to the static magnetic field @ 10 kHz.

V_{IN} (V)	I_{IN}(mA)	Magnetic Flux Density (mT)	V_L (mV) for *B//n*	V_L (mV) for *B⊥n*
3.36	10	0	27	34
3.36	10	400	28	34
3.36	10	600	29	34
3.36	10	800	29	34
3.36	10	1000	29	34

The fig.5.1 and fig.5.2 show the output voltage (V_L), measured when VCSEL was exposed to the static magnetic field oriented ***B//n***. When the magnetic flux density increased, the output voltage increased at both frequencies. The magnetic field affected the current flow within and around an active layer of VCSEL, and the charge carrier density increased in the active region and resulted increasing in optical signal intensity [18]. Proportionally the output voltage increased. For $B \perp n$, when the flux density increased, V_L remained constant at both frequencies, as observed by [18].

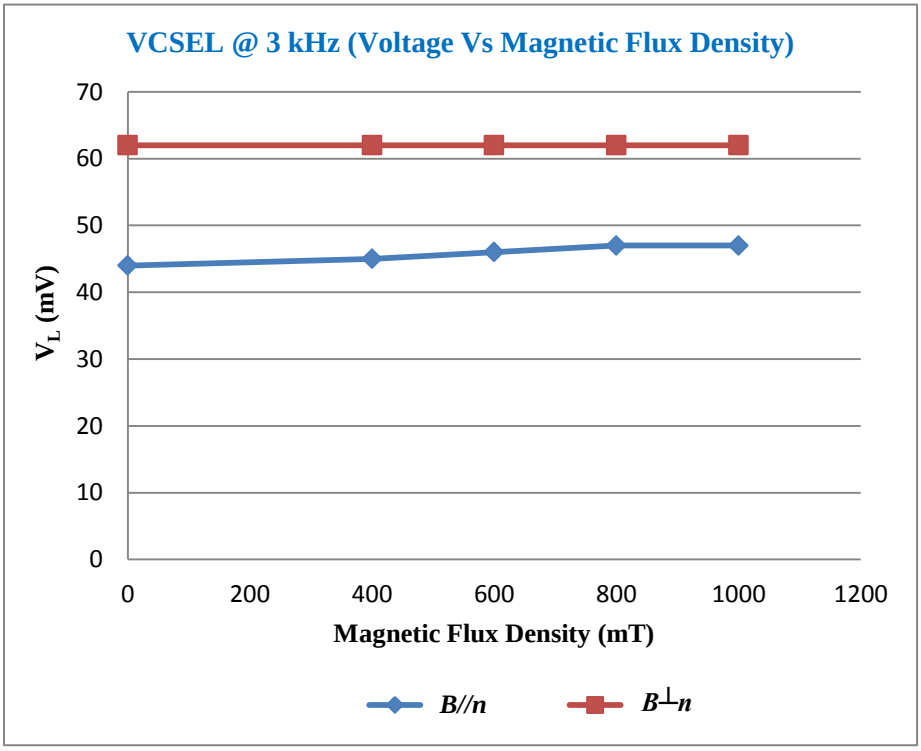

5.1: VCSEL exposed to magnetic field @ 3 kHz (V_L Vs ***B***).

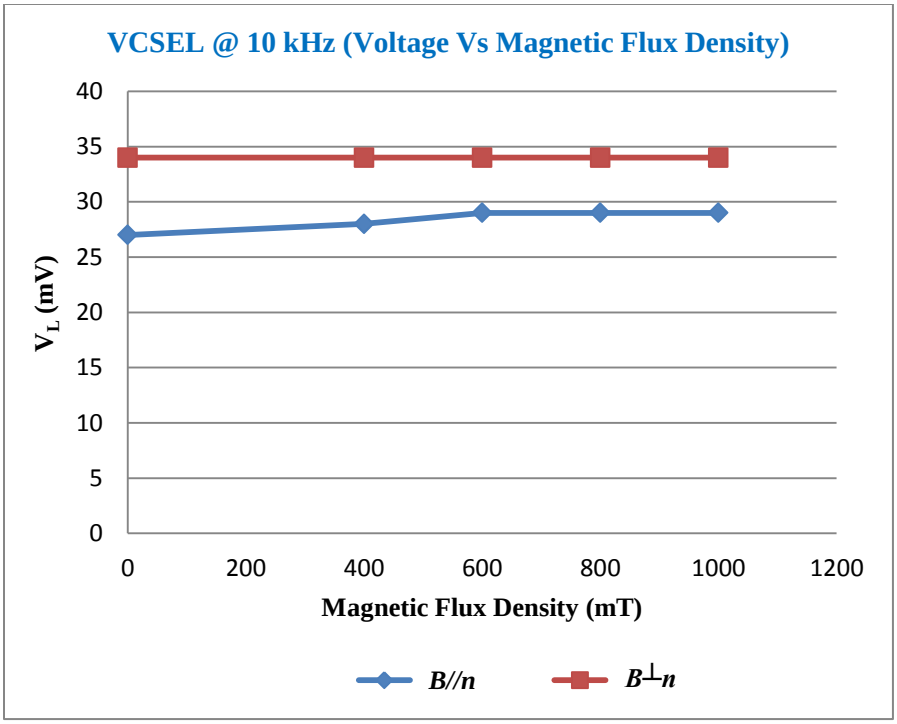

Figure 5.2: VCSEL exposed to magnetic field @ 10 kHz (V_L Vs ***B***).

To demonstrate the magnetic field effect on the output signal when the photodiode was exposed, the experiment was conducted by exposing the PIN photodiode to the static magnetic field oriented ***B//n*** and ***B⊥n***. Then output voltage (V_P) was measured and recorded at different magnetic flux densities and frequencies, as shown in tables 5.3 and 5.4.

Table 5.3: Output Voltage measured when PIN photodiode exposed to the static magnetic field @ 3 kHz.

V_{IN} (V)	I_{IN}(mA)	Magnetic Flux Density (mT)	V_P (mV) for *B//n*	V_P (mV) for *B⊥n*
3.36	8.45	0	59	68
3.36	8.45	400	61	70
3.36	8.45	600	62	72
3.36	8.45	800	63	74
3.36	8.45	1000	63	77

Table 5.4: Output Voltage measured when PIN photodiode exposed to the static magnetic field @ 10 kHz.

V_{IN} (V)	I_{IN}(mA)	Magnetic Flux Density (mT)	V_P (mV) for *B//n*	V_P (mV) for *B⊥n*
3.36	10	0	36	40
3.36	10	400	37	42
3.36	10	600	38	43
3.36	10	800	38	44
3.36	10	1000	38	45

The output voltage (V_P) measured for both ***B//n*** and ***B⊥n*** showed that V_P increased when the magnetic flux density increased at both frequencies, as shown in fig.5.3 & fig.5.4. The charge carriers in the PIN photodiode active region gained energy due to the magnetic field effect and contributed increasing in photocurrent [22], and that resulted rising in V_P.

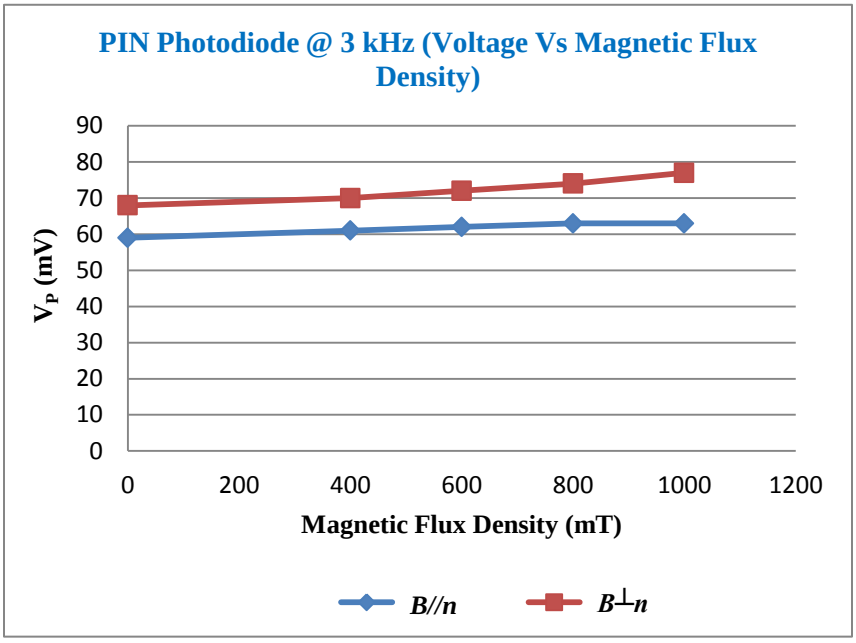

Figure 5.3: PIN photodiode exposed to magnetic field @ 3 kHz (V_P Vs ***B***).

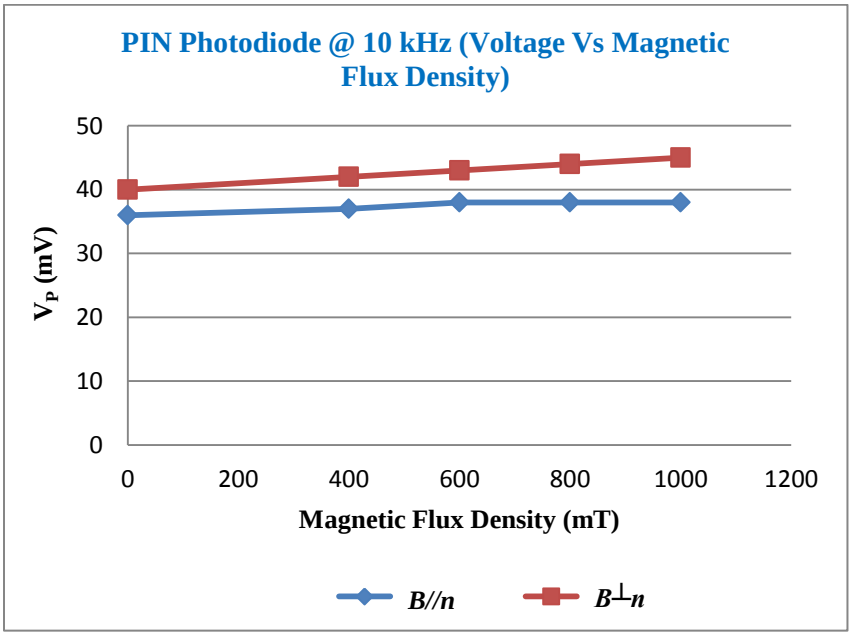

Figure 5.4: PIN photodiode exposed to magnetic field @ 10 kHz (V_P Vs ***B***).

To analyze the difference in the magnetic field effects on the output signal, when laser and photodiode concurrently exposed to the magnetic field relative to individually exposed, both VCSEL and PIN photodiode were simultaneously subjected to the static magnetic field oriented ***B//n*** in the experimental setup. Then the output voltage was measured and recorded at different magnetic flux densities and frequencies, as shown in table 5.5 and 5.6.

Table 5.5: Output Voltage measured when both VCSEL and PIN photodiode concurrently exposed to the static magnetic field @ 3 kHz.

V_{IN} (V)	I_{IN}(mA)	Magnetic Flux Density (mT)	V_{LP} (mV) for ***B//n***
3.36	8.45	0	66
3.36	8.45	400	81
3.36	8.45	600	96
3.36	8.45	800	108
3.36	8.45	1000	113

Table 5.6: Output Voltage measured when both VCSEL and PIN photodiode concurrently exposed to the static magnetic field @ 10 kHz.

V_{IN} (V)	I_{IN}(mA)	Magnetic Flux Density (mT)	V_{LP} (mV) for ***B//n***
3.36	10	0	39
3.36	10	400	49
3.36	10	600	56
3.36	10	800	63
3.36	10	1000	65

The following fig.5.5 and fig.5.6 show the output voltage (V_{LP}) measured when both VCSEL & PIN photodiode concurrently subjected to the magnetic field oriented ***B//n*** at 3 kHz and 10 kHz. The result showed that V_{LP} increased when the magnetic flux densities increased at both frequencies. The charge carrier densities increased in the VCSEL active region due to the magnetic field effect, and that resulted increasing in optical signal intensity [18] as well as the charge carriers in PIN photodiode active region gained energy as a result of the magnetic field effect and contributed to increasing photocurrent [22]. Those combinational effects on VCSEL and PIN photodiode caused increasing in V_{LP} much higher relative to both transducers individually exposed.

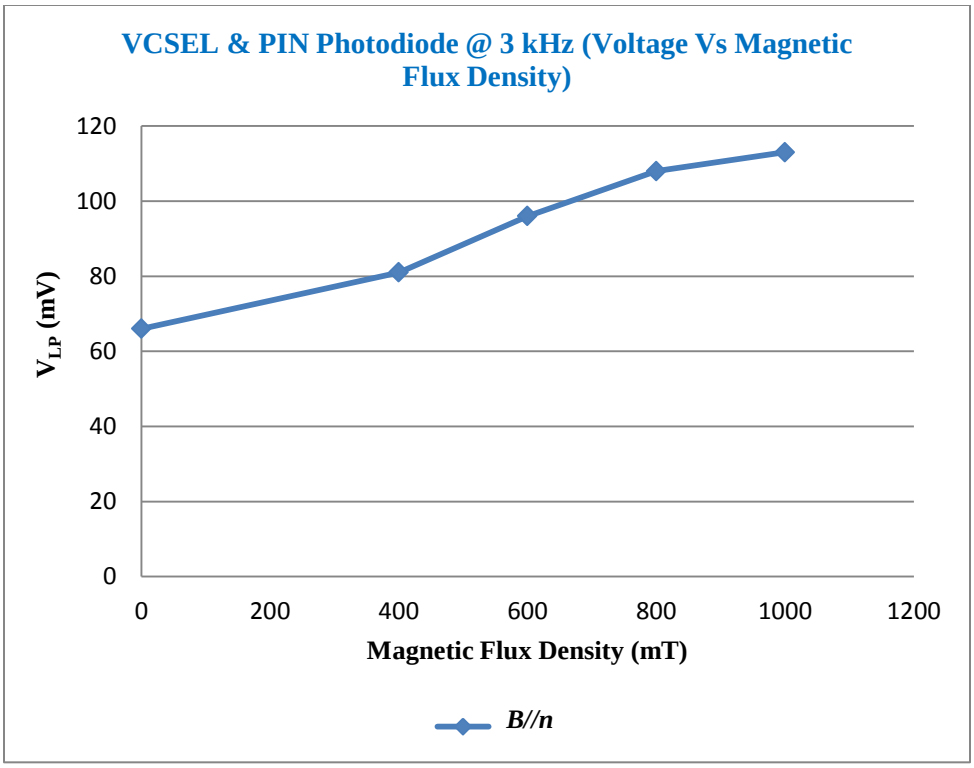

Figure 5.5: Both VCSEL and PIN Photodiode concurrently exposed @ 3 kHz (V_{LP} Vs ***B***).

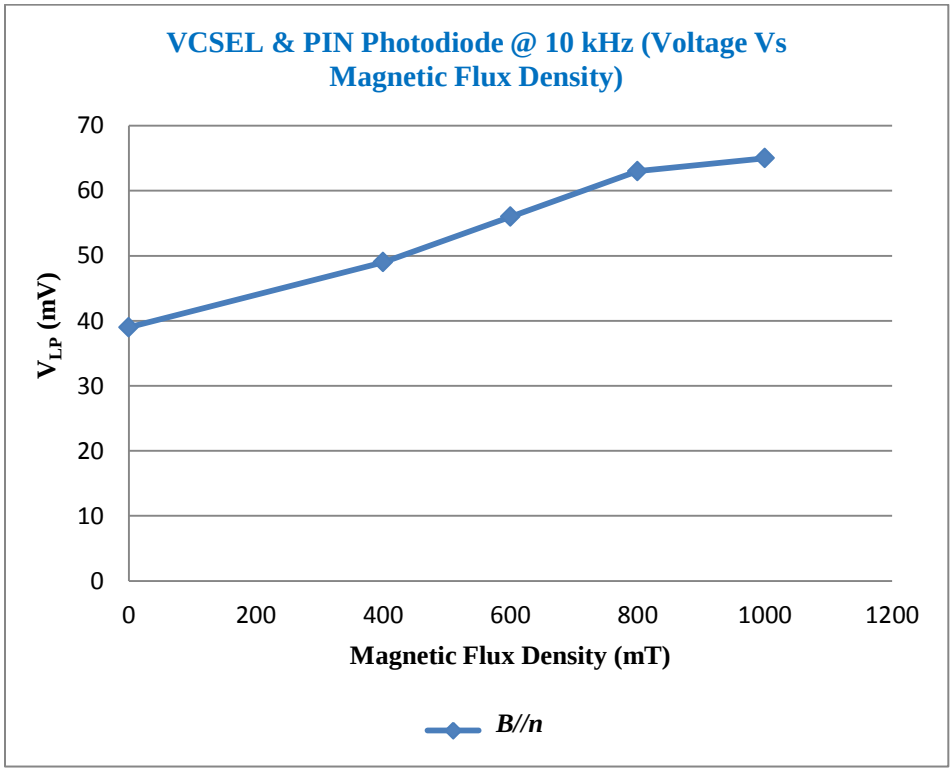

Figure 5.6: Both VCSEL and PIN Photodiode concurrently exposed @ 10 kHz (V_{LP} Vs ***B***).

5.2. Comparison of Magnetic Field Effect on Output Signal at Different Frequencies

The difference in the initial value of output voltage V_L measured at 0T for both ***B//n*** & ***B⊥n*** arrangement at 3 kHz & 10 kHz came from the frequency effect. During experimentation, VCSEL supplied 8.5mA at 3 kHz and 10mA at 10 kHz due to the laser driver arrangement. At a fixed frequency, when the input current feed to VCSEL increases, the optical signal intensity increase [19], and that causes to increase in the output voltage. However, the initial value of output voltage measured at 0T was smaller at 10 kHz relative to 3 kHz due to the frequency effect even with 1.55mA addition in current supplied to VCSEL at 10 kHz. Similar influences occurred in both V_P and V_{LP}. However, the objective of this study was not to compare the initial value of voltage measured. It was to compare the rate of changes in output voltage due to the magnetic field effect at different frequencies. Even with those differences in the initial values, it was possible to identify the rate of change in output voltage, and comparisons were made.

To study the influence of change in input signal frequency to the magnetic field effect on the output signal when laser and photodiode individually and concurrently exposed to the field, the change in output voltage (ΔV_L, ΔV_P, and ΔV_{LP}) at different flux densities and frequencies were compared. The upper case delta (Δ) donated the change in output voltage values when the magnetic flux densities varied from 0 to 400, 600, 800, and 1000mT. To calculate the ΔV_L, ΔV_P, and ΔV_{LP}, the output voltage (V_L, V_P, and V_{LP}) measured at 0T were used as a reference.

5.2.1. VCSEL Exposed to Magnetic Field

The output voltage measured from the experimental setup exposing VCSEL to the static magnetic field at different magnetic flux densities and frequencies were compared to study the effects. The comparisons were made based on the rate of change in output voltage (ΔV_L) when the magnetic flux density varied from 0 to 400mT, 600mT, 800mT, and 1000mT at 3 kHz and 10 kHz for ***B//n*** as shown in the following table 5.7.

Table 5.7: Comparison of magnetic field effect on output voltage at different frequency when VCSEL exposed to magnetic field oriented ***B//n***.

Change in Magnetic Flux Density (mT)	**ΔV_L (mV) @ 3 kHz**	**ΔV_L (mV) @10 kHz**
0 to 400	1	1
0 to 600	2	2
0 to 800	3	2
0 to 1000	3	2

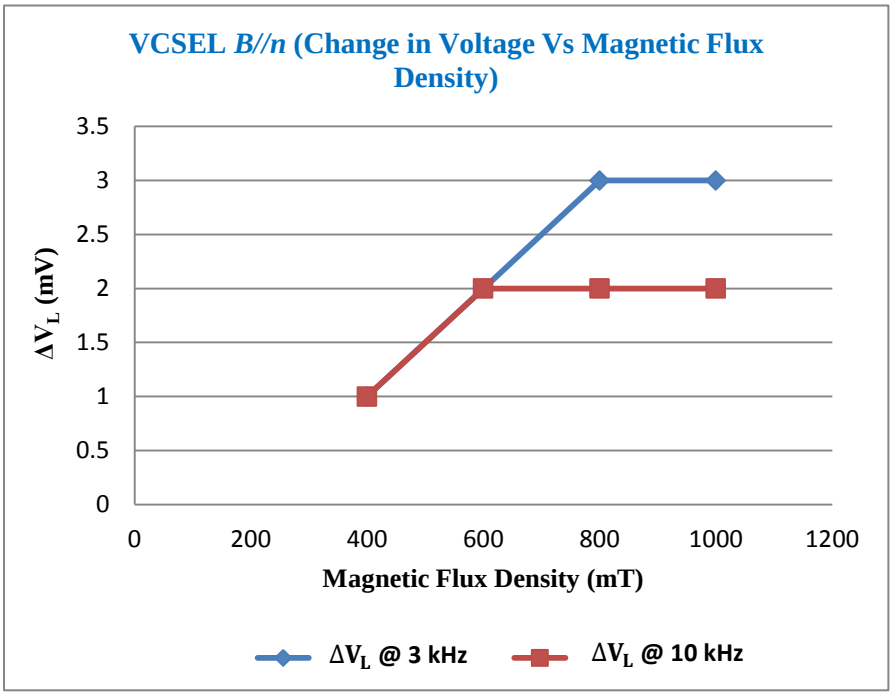

Figure 5.7: Comparison of ΔV_L at 3 kHz & 10 kHz when VCSEL exposed to magnetic field oriented ***B//n***.

As shown in the above fig.5.7, at 3 kHz, when the magnetic flux density increased from 0T to 1000mT the ΔV_L increased by 3mV. However, the frequency increased to 10 kHz, ΔV_L increased by only 2mV when magnetic flux density increased from 0T to 1000mT. The overall change in output voltage at 3 kHz was higher by 1mV than at 10 kHz. That indicated the effect of magnetic field on output signal when VCSEL exposed to the magnetic field higher at 3 kHz than at 10 kHz.

5.2.2 PIN Photodiode Exposed to Magnetic Field

To identify the influence of change in input signal frequency to the magnetic field effect on output signal when photodiode exposed, the rate of change in output voltage (ΔV_P) measured from the experimental setup when PIN photodiode exposed to the magnetic field were compared. The comparisons were made based on the ΔV_P when the magnetic flux density varied from 0 to

400mT, 600mT, 800mT, and 1000mT; for ***B//n*** and ***B⊥n*** at 3 kHz & 10 kHz, as shown in table 5.8 and 5.9.

Table 5.8: Comparison of magnetic field effect on output voltage at different frequency when PIN photodiode exposed to magnetic field oriented ***B//n***.

Change in Magnetic Flux Density (mT)	**ΔV_P (mV) @ 3 kHz**	**ΔV_P (mV) @ 10 kHz**
0 to 400	2	1
0 to 600	3	2
0 to 800	4	2
0 to 1000	4	2

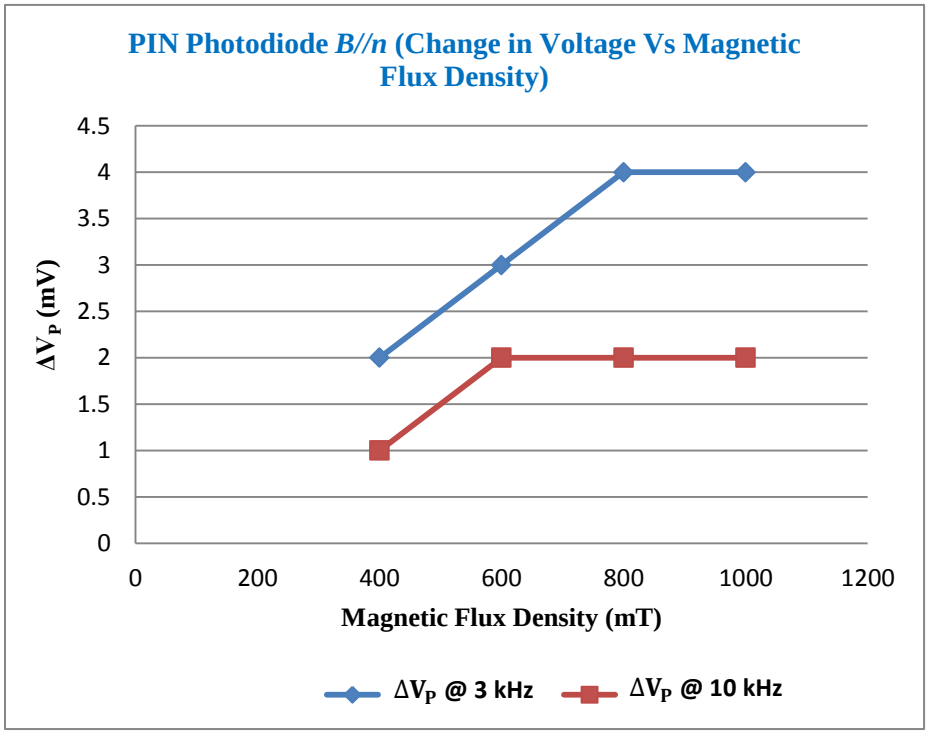

Figure 5.8: Comparison of ΔV_P at 3 kHz & 10 kHz when PIN photodiode exposed to magnetic field oriented ***B//n***.

For ***B//n***, at 3 kHz, the change in output voltage (ΔV_P) increased by 4mV when the magnetic flux density increased from 0T to 100mT, as shown in fig.5.8. But, the frequency increased to 10 kHz, the ΔV_P augmented by 2mV for the same magnetic flux density. So, overall ΔV_P at 3 kHz was higher by 2mV than at 10 kHz. The result showed that the magnetic field effect on the output signal was higher at 3 kHz than 10 kHz when the PIN photodiode was subjected to the magnetic field.

Table5. 9: Comparison of magnetic field effect on output voltage at different frequency when PIN photodiode exposed to magnetic field oriented $\boldsymbol{B^{\perp}n}$.

Change in Magnetic Flux Density (mT)	ΔV_P (mV) @ 3 kHz	ΔV_P (mV) @ 10 kHz
0 to 400	2	2
0 to 600	4	3
0 to 800	6	4
0 to 1000	9	5

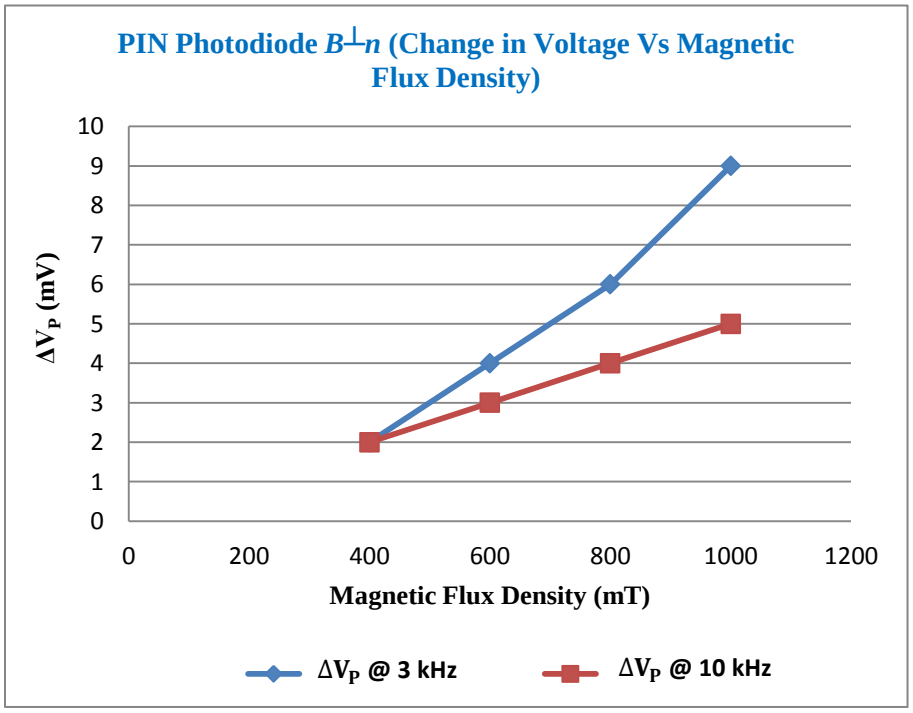

Figure 5.9: Comparison of ΔV_P at 3 kHz & 10 kHz when PIN photodiode exposed to magnetic field oriented $\boldsymbol{B^{\perp}n}$.

Similarly, for $\boldsymbol{B^{\perp}n}$, the rate of change in output voltage (ΔV_P) at 3 kHz increased by 9mV when the magnetic flux density increased from 0T to 1000mT, as shown in the above fig.5.9. However, when the frequency increased to 10 kHz the ΔV_P increased by only 5mV. The total ΔV_P at 3 kHz was higher by 4mV than at 10 kHz. So, the influence of magnetic field effect on output signal was also greater at 3 kHz than 10 kHz when PIN photodiode subjected to the magnetic field oriented $\boldsymbol{B^{\perp}n}$.

5.2.3 VCSEL and PIN Photodiode Concurrently Exposed to Magnetic Field

To analyze the impact of change in the input signal frequency to the magnetic field effect on output signal when laser and photodiode concurrently subjected, the rate of change in output voltage (ΔV_{LP}) at 3 kHz & 10 kHz were compared. The comparisons were made based on the

amount of change in output voltage when magnetic flux density oriented ***B//n*** varied 0 to 400mT, 600mT, 800mT, and 1000mT at both frequencies, as shown in table 5.10.

Table 5.10: Comparison of magnetic field effect on output voltage at different frequency when both VCSEL and PIN photodiode simultaneously exposed to magnetic field oriented ***B//n***.

Change in Magnetic Flux Density (mT)	**ΔV_{LP} (mV) @ 3 kHz**	**ΔV_{LP} (mV) @ 10 kHz**
0 to 400	15	10
0 to 600	30	17
0 to 800	42	24
0 to 1000	47	26

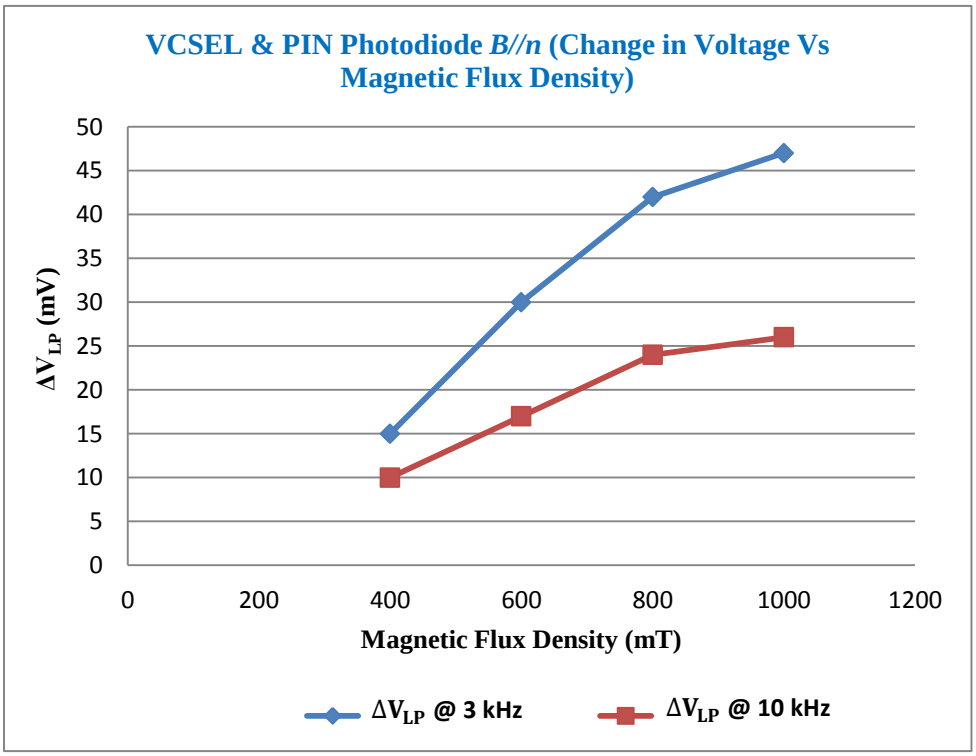

Figure 5.10: Comparison of ΔV_{LP} at 3 kHz & 10 kHz when both VCSEL and PIN photodiode exposed to magnetic field oriented ***B//n***.

For both VCSEL and PIN photodiode concurrently exposed to the magnetic field, the change in output voltage (ΔV_{LP}) increased by 47mV at 3 kHz and 26mV at 10 kHz when magnetic flux density increased from 0T to 1000mT at both frequencies, as shown in fig.10. The overall ΔV_{LP} at 3 kHz was higher by 21mV than at 10 kHz. The results showed that the magnetic field effect on output signal when VCSEL and PIN photodiode concurrently exposed to the magnetic field was higher at 3 kHz than at 10 kHz.

5.3 Comparison of Magnetic Field Effect on Output Signal VCSEL and PIN Photodiode Individually and Concurrently Exposed at Fix Frequency

To study the difference in the magnetic field effect on the output signal at a fixed frequency when laser and photodiode concurrently exposed to the magnetic field relative to individually exposed, the rate of change in output voltage was compared. The following table 5.11 & 5.12 show the amount of change in output voltage ΔV_L, ΔV_P & ΔV_{LP} when VCSEL and PIN photodiode individually and concurrently exposed to the magnetic field oriented ***B//n*** at 3 kHz and 10 kHz.

Table 5.11: Comparison of magnetic field effect on output voltage when both VCSEL and PIN photodiode individually and simultaneously exposed to magnetic field oriented ***B//n*** @ 3 kHz.

Change in Magnetic Flux Density (mT)	**ΔV_L (mV)**	**ΔV_P (mV)**	**ΔV_{LP} (mV)**
0 to 400	1	2	15
0 to 600	2	3	30
0 to 800	3	4	42
0 to 1000	3	4	47

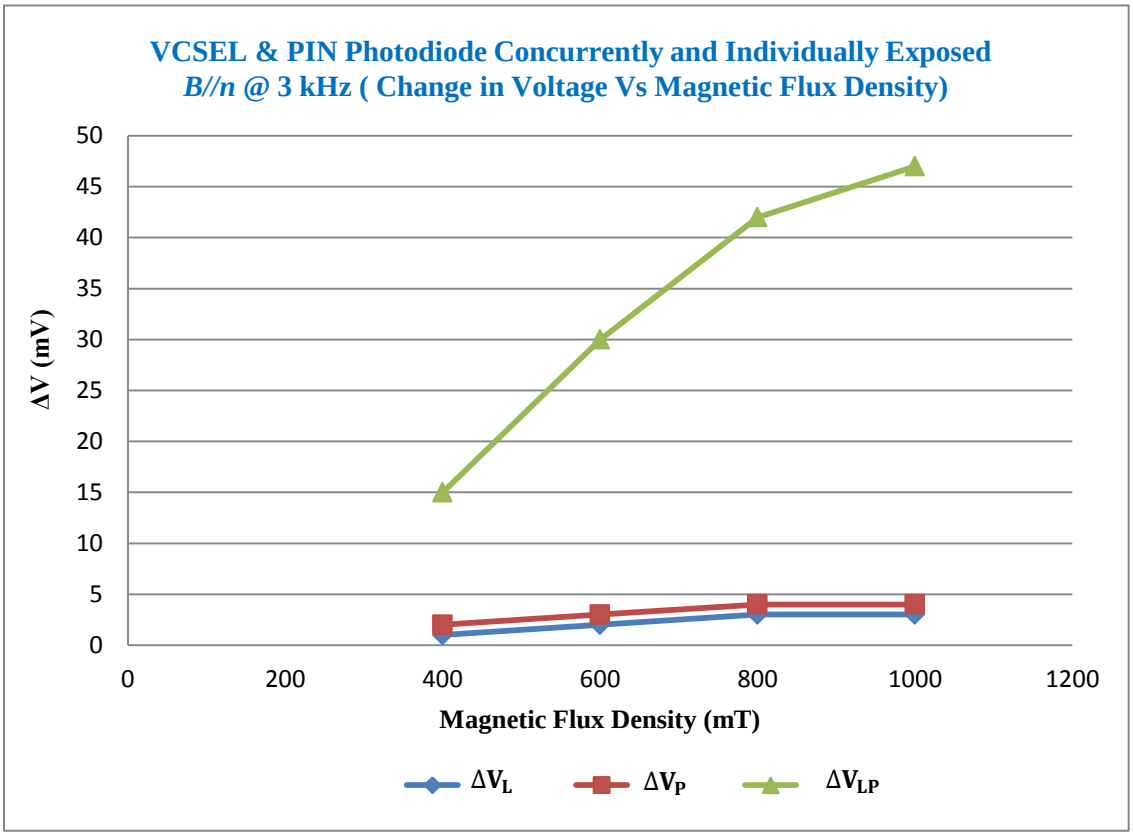

Figure 5.11: Comparison of ΔV_L, ΔV_P, and ΔV_{LP} at 3 kHz for ***B//n***.

As shown in the above fig.5.11, at 3 kHz, when the magnetic flux density increased from 0T to1000mT, the overall change in output voltage ΔV_L increased by 3mV, ΔV_P increased by 4mV, and ΔV_{LP} increased by 47mV. The results indicated that the rate of magnetic field effect on output signal when the VCSEL and PIN photodiode concurrently expose to the field was much higher than separately subjected. The magnetic field caused increasing in V_L and V_P when both transducers were individually exposed. But, the contribution of magnetic file effect on output voltage was relatively much higher when both VCSE and PIN photodiode were concurrently subjected to the magnetic field.

Table 5.12: Comparison of magnetic field effect on output voltage when both VCSEL and PIN photodiode individually and simultaneously exposed to magnetic field oriented ***B//n*** @ 10 kHz.

Change in Magnetic Flux Density (mT)	**ΔV_L (mV)**	**ΔV_P (mV)**	**ΔV_{LP} (mV)**
0 to 400	1	1	10
0 to 600	2	2	17
0 to 800	2	2	24
0 to1000	2	2	26

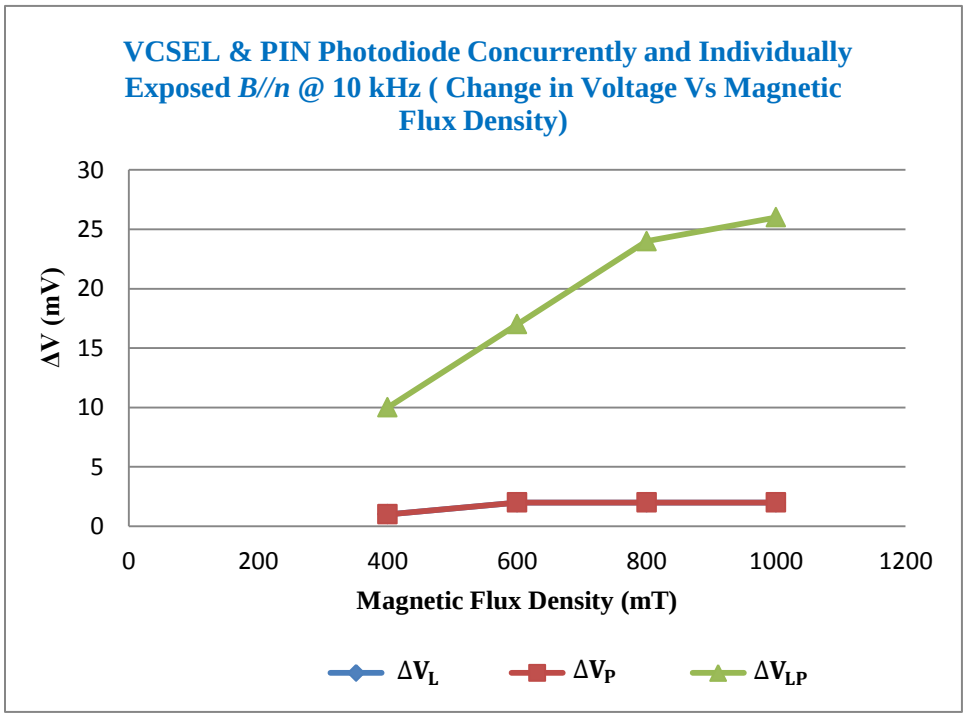

Figure 5.12: Comparison of ΔV_L, ΔV_P, and ΔV_{LP} at 10 kHz for ***B//n***.

In the above fig 5.12, the blue line represented ΔV_L in the graph is hidden behind the brown line because ΔV_L and ΔV_P have the same values. So, it is important to consider still there. Similarly,

at 10 kHz, when magnetic flux density increased from 0T to 1000mT, ΔV_L increased by 2mV, ΔV_P increased by 2mV, and ΔV_{LP} increased by 26mV. That indicated the contribution of the magnetic field on the output signal when the VCSEL and PIN photodiode concurrently exposed was much higher than individually exposed.

Chapter 6

Conclusion and Future Works

6.1 Conclusion

In this thesis work, experimentation-based analyses were made to identify the influence of change in input signal frequency to the magnetic field effect on output signal when both laser and photodiode are concurrently and separately exposed to the magnetic field. Additionally, the differences in magnetic field effect on the output signal when laser and photodiode are concurrently exposed to the magnetic field relative to individually exposed were analyzed. The experimentation was made by exposing 850nm VCSEL and PIN photodiode up to 1000mT magnetic flux density at around room temperature.

The results were compared based on the rate of change in output voltage measured at different magnetic flux densities and frequencies. For ***B//n***, when the magnetic flux densities increased from 0 to 1000mT, the ΔV_L, ΔV_P, and ΔV_{LP} were higher by 1mV, 2mV, and 21mV respectively at 3 kHz compared to at 10 kHz. Similarly, for $\boldsymbol{B \perp n}$, when magnetic flux density increased from 0 to 1000mT, the ΔV_P was higher by 4mV at 3 kHz compared to at 10 kHz, but ΔV_L remained constant at both frequencies. The overall results showed that when the input signal frequency increased from 3 kHz to 10 kHz, the magnetic field effect on the output signal decreased for both VCSEL and PIN photodiode individually and concurrently exposed to the magnetic field except when VCSEL was exposed $\boldsymbol{B \perp n}$ orientation. For magnetic field aligned parallel to VCSEL's layered surface, no change in output signal was observed.

The comparisons carried out at a fixed frequency for ***B//n***, at 3 kHz, showed that when magnetic flux density increased from 0 to 1000mT, the ΔV_L, ΔV_P, and ΔV_{LP} increased by 3mV, 4mV, and 47mV, respectively. Similarly, at 10 kHz, the ΔV_L, ΔV_P, and ΔV_{LP} increased by 2m, 2mV, and 21mV, respectively. Based on the results from comparisons taken, the contribution of magnetic field effect on output signal was found much higher when both VCSEL and PIN photodiode were concurrently exposed compared to individually exposed at both 3 kHz and 10 kHz.

6.2 Future Works

This thesis focused on the effect of change in input signal frequency to the magnetic field effect on output signal when laser and photodiode individually and concurrently exposed. Additionally,

the difference in magnetic field effect on the output signal when both laser and photodiode simultaneously exposed relative to individually exposed was analyzed. The experiments were conducted by connecting VCSEL and PIN photodiode with other materials in the experimental setup to study the effects. However, some experiments were conducted by repositioning the VCSEL and PIN photodiode in the setup. There was a difference in optical signal loss during coupling from laser to photodiode from experiment to experiment and has a certain impact on the accuracy of results for comparisons purpose even though comparisons were possible with those effects. In future work, the experiments conducted by placing laser and detector at a fixed position will give a more accurate result suit for comparisons.

Moreover, the input current supplied to VCSEL at 3 kHz was 8.5mA, and at 10 kHz was supplied 10mA due to laser driver arrangement. Even though the effects were able to observe with different input currents, the experiments conducted supplying the same input current to VCSEL at both frequencies will have a more visible difference in the output signal which results due to the magnetic field effect.

Furthermore, the experimentation was made using only VCSEL and PIN photodiode. However, in the photon-electron interfaces, different types of lasers and photodiodes are being used. The effects also depend on the transducers type. So, in future work, the experimentation using the other type of transducers used in photon-electron interfaces are expected.

References

[1] https://www.allaboutcircuits.com/textbook/semiconductors/chpt-13/early-tube-history/, 11:15Am, 11/23/2019.

[2] https://www.cedmagic.com/history/transistor-1947.html, 10:30Am, 11/23/2019.

[3] R. N. Noyce, "Microelectronics," *Scientific American*, vol. 237, no. 3, pp. 62-69, 1977.

[4] S. E. Thompson and S. Parthasarathy, "Moore's law: the future of Si microelectronics," Materials today, vol. 9, no. 6, pp. 20-25, 2006.

[5] A. Mahendra, "Electronic Photonic Integrated Circuits and Control Systems," Ph.D. dissertation, Dept. Elect. & Comput. Eng., Univ. Sydney, Sydney, Australia, 2018.

[6] S. Chih-Tang, "Evolution of the mos transistor-from conception to vlsi," *Proceedings of the IEEE,* vol. 76, no. 10, pp. 1280-1326, 1988.

[7] A. E. Dunlop, W. J. Evans, and L. A. Rigge, "Managing complexity in ic design-past, present, and future," *Bell Labs technical journal*, vol. 2, no. 4, pp. 103-125, 1997.

[8] G. E. Moore, "Intel: Memories and the microprocessor," Daedalus, pp. 55-80, 1996.

[9] [Online]. Available: https://www.qualcomm.com/news/releases/2016/11/17/ Qualcomm - and-samsung-collaborate-10nm-process-technology-latest-snapdragon

[10] I. S. Amiri, et al., "Introduction to photonics: Principles and the most recent applications of microstructures," *Micromachines*, vol. 9, no.9, pp. 1-25, 2018.

[11] N. Savage, "Linking with light [high-speed optical interconnects]," *Spectrum, IEEE*, vol. 39, no. 8, pp. 32-36, 2002.

[12] C. Batten, A. Joshi, J. Orcutt, A. Khilo, B. Moss, C. Holzwarth, M. Popovic, H. Li, H. I. Smith, J. Hoyt et al., "Building manycore processor-to-dram networks with monolithic silicon photonics," in *High Performance Interconnects*, 2008. HOTI'08.16th IEEE Symposium on. IEEE, 2008, pp. 21-30.

[13] Sergiusz Patela, Photonics devices Introduction, Wrocław University of Technology Wrocław, Poland Sergiusz.Patela@pwr.wroc.pl, 2005.

[14] L. Chrostowski and M. Hochberg, Silicon Photonics Design: From Devices to Systems. Cambridge University Press, 2015.

[15] V. J. Sorger, et al., "Toward integrated plasmonic circuits," *MRS bull*, vol.*37*, no.8, 2012, pp.728-738.

[16] L. C. Kimerling et al., "Electronic-photonic integrated circuits on the CMOS platform,"

In *Silicon photonics*, vol. 6125, p. 612502, SPIE, 2006.

[17] G. Q. Lo, K. W. Ang, T. Y. Liow, Q. Fang, J. Zhang, S. Y. Zhu, et al., "Silicon Photonics Technologies for Monolithic Electronic-Photonic Integrated Circuit," in ECS Transactions, 11 Science Park Road, Singapore, 2010, Paper 117685.

[18] Y. Yamagishi, et al., "Oscillation wavelength shifts observed in vertical cavity surface emitting lasers exposed to magnetic fields," *Phys. Simul. Optoelectron. Devices*, vol. 8255, SPIE, 2012.

[19] J. Troska, et al., "Laser and photodiode environmental evaluation for the Versatile Link project," *J. Instrum.*, pp. 1- 9, Feb. 2013.

[20] T. A. Zaker and A. K. Hafiz, "Influence of Magnetic Field on the Threshold Current, Temperature Characteristics , and on the Output Power in AlGaInP Multiple Quantum Well Laser," *Appl. Phys. Res.*, vol. 3, no. 2, pp. 143-151, Nov. 2011.

[21] S. H. Zyoud and A. Abdelkader, "The Influence of Magnetic Field on Pulse Distribution of Laser Diode," *Univers. J. Electr. Electron. Eng.*, vol. 6, no.5, pp. 323-328, Dec. 2019, doi: 10.13189/ujeee.2019.060503.

[22] S. A. Elhouri and M.D. Abd-Alla, "Responsivity of Silicon Photodiodes Light and Dark Current under Influence of Different Magnetic Flux," *J. Appl. Ind. Sci.*, vol. 1, no. 5, pp. 10-16, Dec. 2013.

[23] Optoelectronic Devices and Materials, Springer International Publishing AG, New York, NY, USA, 2017, pp. 900 - 917.

[24] https://www.thorlabs.de/NewGroupPage9_PF.cfm?ObjectGroup_ID=1832, 10:20Am, 11/20/2019.

[25] https://www.fiberlabs.com/glossary/about-semiconductor-laser-diode/, 8:35Am, 11 /15/2019.

[26] K. Iga, "Vertical-cavity surface-emitting laser: Its conception and evolution", *Jpn. J. Appl. Phys.*, vol. 47, no. 1, pp. 1- 6, 2008.

[27] https://www.lightreading.com/distributed-feedback-(dfb)-lasers/d/d-id/575160, 10:20Am, 12/20/2019.

[28] B. Saleh and M. C. Teich, "Fundamentals of Photonics," *Madison, Wisconsin, USA:* John Wiley & Sons, Inc., 1991.

[29] S. M. Sze, "Photonic Devices," in *Semiconductor Devices Physics and Technology*, 2nd ed.,

vol. 23, no.1, New York, NY: John Wlley & Sons, Inc., 2002, pp. 309-311.

[30] https://www.chem.uci.edu/~unicorn/old/H2A/handouts/PDFs/RWFQWells.pdf, 10:00Am, 11/ 18/2019.

[31] G. P. Agrawal, "Optical Receivers," *in Fiber-Optic Communications System*, 3rd ed. New York, NY, USA: Wiley, 2002, pp. 133-144.

[32] S. Yoshida, Y. Tada, I. Kotaka, and K. Wakita, "InGaAlAs/InAlAs multiquantum well electro absorption phase modulator module," *Electronics Letters*, vol. 30, no. 21, pp.1795-1796,1994.

[33] N. Yoshimoto, et al., "InGaAlAs/InAlAs multiple quantum well phase modulator integrated with spot size conversion structure," *IEEE photonics technology letter*, vol. 6, no.2, pp. 208 210,1994.

[34] J. M. Senior, "Transmission characteristics of optical fibers," in *Optical Fiber Communications Principles and Practice*, 3rd ed., Harlow: Pearson Education Limited, 2009, pp. 87-151.

[35] https://www.ikbooks.com/home/samplechapter?filename=190_Sample-Chapter.pdf, 11:10Am, 2/25/2019.

[36] D. Axelrod, et al., "Total internal reflection fluorescence," Annual review of biophysics and bioengineering, vol.13, no.1, 1984, pp. 247-268.

[37] P. Sharma, et al., "Fibre Optic Communications : An Overview", *Int. J. Emerg. Technol. Adv. Eng.*, vol. 3, no. 5, pp. 474-479, May 2013.

[38] B. Saleh and M. Carl Teich, "FIBER OPTICS," in *Fundamental of Photonics*, vol. 5, New York, NY: John Wiley & Sons, Inc., 1991, pp. 272-302.

[39] M. Arumugam, "Optical Fibre Communication - An Overview," *Pramana journal of physics*, vol. 57, Nos5 & 6, PP. 849-869, 2001.

[40] J. Ahmed et al., "Advancements in Silicon Photonics," in *Optical Signal Processing by Silicon Photonics*, Springer Briefs in Materials, 2013, pp. 33-49.

[41] http://www-eng.lbl.gov/~shuman/NEXT/CURRENT_DESIGN/TP/FO/Lect4-Optical% 20 waveguides.pdf, 10:40Am, 25/20/2019.

[42] M. Nasir Uddin, et al., "Performance Analysis of Different Loss Mechanisms in Optical Fiber Communication," *Comput. Appl. An Int. J.*, vol. 2, no. 2, pp. 1-13, May 2015.

[43] P. K. Dubey and V. Shukla, "Dispersion in Optical Fiber Communication," *Int. J. Sci. Res.*,

vol. 3, no. 10, pp. 236-237, Oct. 2014.

[44] E. Çerri, "The Effect of PMD (Polarization Mode Dispersion) the Fibers of New and Old In Different Distance in Numerical Systems with Optical Fiber WDM," *Int. J. Eng. Sci. Invent.*, vol. 5, no. 8, pp. 62-63, Aug. 2016.

[45] http://opti500.cian-erc.org/opti500/pdf/sm/Module3%20Optical%20Attenuation.pdf, 8:20Am, 2/11/2020.

[46] http://www.eng.ucy.ac.cy/ece455/docs/Lectures/07_Optical_Fibre_Attenuation_ECE455_2016.pdf, 9:25Am, 3/10/2020.

[47] Dr. A. Satapathy and Er. S. K. Padhan, "Signal Attenuation In Optical Fibers and its Remedies," *Int. J. Instrum. Electr. Electron. Eng.*, vol. 1, no.3, pp. 26-30, May 2013.

[48] https://www.fiberoptics4sale.com/blogs/archive-posts/95048006-optical-fiber loss-andatten uation#:~:text=For%20glass%20fibers%2C%20Mie%20scattering,the%20fiber%2C%20or%20diameter%20fluctuations, 8:45Am, 2/10/2020.

[49] A. Boh Rffin, "Stimulated brillouin scattering: an overview of measurements, system impairments, and applications," In *Technical Digest: Symposium on Optical Fiber Measurements,* Vol. 2004, pp. 23-28, 2004.

[50] N. Kaur and H. S. Parmar, "Non-linear scattering effects in fiber optic cables: a comprehensive review," *Int. J. Sci. Eng. Res.*, vol. 7, no. 11, pp. 217-226, Nov. 2016.

[51] M. M. Ramsay and G. A. Hockham, "Propagation in optical fiber waveguides," *in Optical Fiber Communication Systems, C. P. Sandbank, Ed.* New York, NY, USA: Wiley, 1980, pp. 25-41.

[52] H. F. Wolf, "Optical waveguides", H. F. Wolf, Ed., Handbook of Fiber Optics: Theory and Applications, New York, USA: Garland STPM Press, 1979, pp. 43-152

[53] W. A. Gambling, et al., "Curvature and micro bending losses in single mode optical fibers," *Opt. Quantum Electron.*, vol. 11, no.3, pp. 43-59, 1979.

[54] B. I. Bakare, et al., "Reduction of Micro Bend Losses in Optical Fibers Reduction of Micro Bend Losses in Optical Fibers," *Eur. J. Adv. Eng. Technol.*, vol. 7, no. 12, pp.1-8, 2020.

[55] http://muree.psut.edu.jo/Project/Puplications/Optical%20losses.pdf, 10:20Am, 4/23/2020.

[56] R.A. Soref, "The past, present, and future of silicon photonics," *IEEE Journal of Selected Topics in Quantum Electronics, vol.*12, no.6, pp.1678-1687, 2006.

[57] R. T. Swimm, “Optical absorption in the band gap in high purity silicon,” in Basic Properties of Optical Materials, Presented at the Topical Conference on Basic Properties of Optical Materials, Vol. OM85, Albert Feldman, Ed. Washington, DC: U.S. Dept. Commerce/National Bureau Standards Spec. Pub. #697, pp. 158-159, 1985.

[58] V. Donzella, et al., “Study of waveguide crosstalk in silicon photonics integrated circuits.,” *Photonics North 2013*, vol. 8915, SPIE, 2013.

[59] T. Barwicz and H.I. Smith, "Evolution of line-edge roughness during fabrication of High-index-contrast microphotonic devices," *Journal of Vacuum Science & Technology B: Microelectronics and Nanometer Structures*, vol, 21, no.6, pp. 2892-2896, 2003.

[60] E. A. Marcatili, "Bends in optical dielectric guides," *Bell Syst. Tech. J.*, vol. 48, no.7, pp. 2103-2132, 1969.

[61] G.P. Agrawal, N.K. Dutta, "Long-wavelength semiconductor lasers," Van Nostrand Reinhold Company, 1986.

[62] S. Blaser, et al. “Terahertz intersub band emission in strong magnetic fields,” *Appl. Phys. Letters*, vol.81, no.1, pp. 67-69, 2002.

[63] A. Yariv and B. Zhao, “Quantum Well Semiconductor Lasers”, In E. Kapon, Ed. Semiconductor Lasers I: Fundamentals, Academic Press, 1999, pp. 1-121.

[64] T. Miyamoto, et al., “An investigation into changes observed in the oscillation characteristics of semiconductor lasers exposed to magnetic fields,” *In Physics and Simulation of Opto-electronic Devices XIV*, International Society for Optics and Photonics, Vol. 6115, 2006.

[65] S. M. Sze, “Physics of Semiconductor Devices,” New York: Wiley, 2001.